

AD-A051 657

UNITED TECHNOLOGIES RESEARCH CENTER EAST HARTFORD CONN

F/G 11/5

EVALUATION OF TANTALUM FIBER REINFORCED SI3N4.(U)

APR 77 J J BRENNAN

N62269-76-C-0104

UNCLASSIFIED

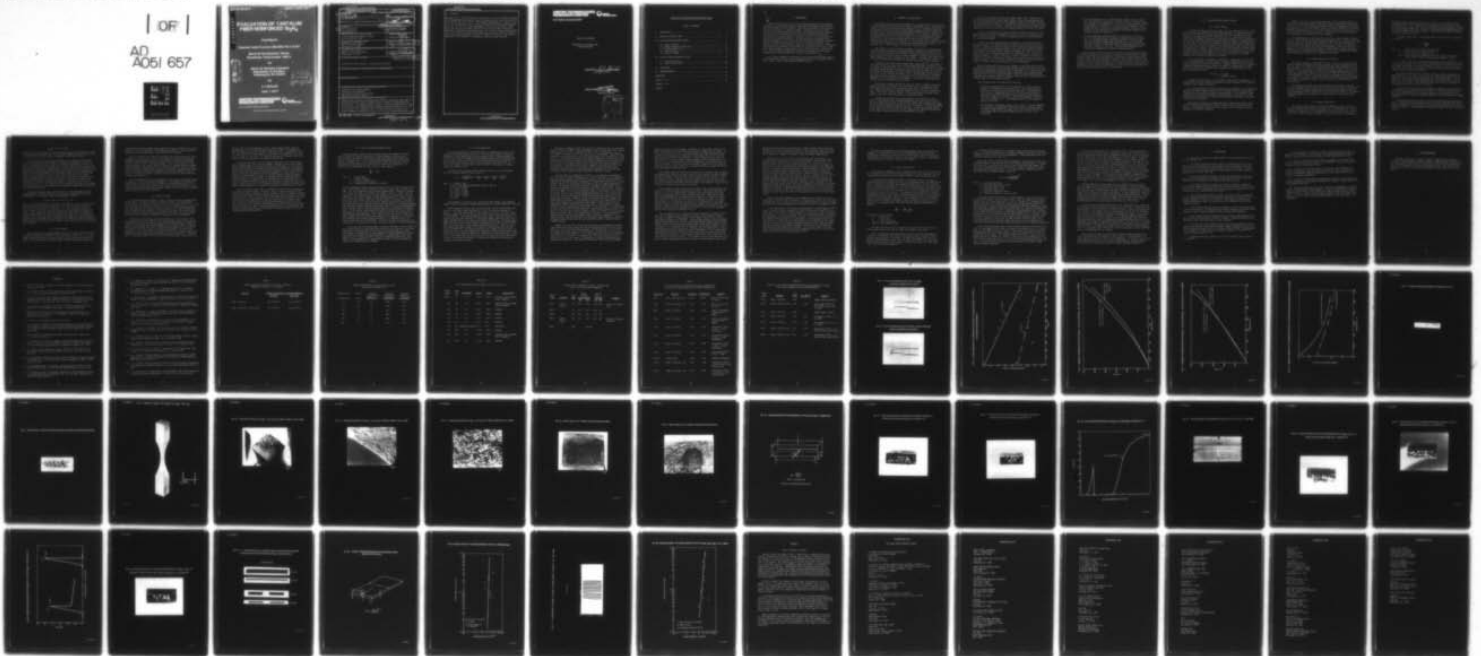
UTRC-R77-912538-4

NADC-75207-30-A

NL

| OF |

AD
A051 657



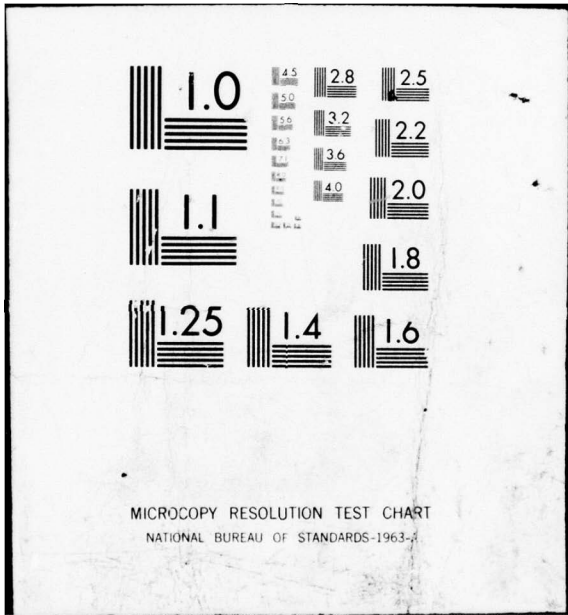
END

DATE

FILMED

4-78

DDC



10

AD A 051 657

EVALUATION OF TANTALUM FIBER REINFORCED Si₃N₄

Final Report

Prepared under Contract N62269-76-C-0104

Naval Air Development Center
Warminster, Pennsylvania 18974

for

Naval Air Systems Command
Department of the Navy
Washington, DC 20361

by

J. J. Brennan

April 1, 1977

AD No. *10*
DDC FILE COPY

DDC
RECEIVED
MAR 23 1978
RECEIVED
JF
A

**UNITED TECHNOLOGIES
RESEARCH CENTER**



UNITED TECHNOLOGIES

EAST HARTFORD, CONNECTICUT 06108

" Approved for public release—Distribution unlimited "

19 REPORT DOCUMENTATION PAGE		READ INSTRUCTIONS BEFORE COMPLETING FORM	
1. REPORT NUMBER NADC-75207-30-A	2. GOVT ACCESSION NO.	3. RECIPIENT'S CATALOG NUMBER 1	
4. TITLE (and Subtitle) EVALUATION OF TANTALUM FIBER REINFORCED Si_3N_4		5. TYPE OF REPORT & PERIOD COVERED Final Report. 1 Mar 1976 - Mar 1977	
7. AUTHOR(s) John J./Brennan	14. UT RC	6. PERFORMING ORG. REPORT NUMBER R77-912538-4	
		8. CONTRACT OR GRANT NUMBER(s) N62269-76-C-0104	
9. PERFORMING ORGANIZATION NAME AND ADDRESS United Technologies Research Center East Hartford, CT 06108		10. PROGRAM ELEMENT, PROJECT, TASK AREA & WORK UNIT NUMBERS A3200000/001A/6R02204001	
11. CONTROLLING OFFICE NAME AND ADDRESS Department of the Navy Naval Air Systems Command Washington, DC 20361		12. REPORT DATE April 1, 1977 1 Apr 77	
14. MONITORING AGENCY NAME & ADDRESS (if different from Controlling Office) Department of the Navy Naval Air Development Center Warminster, PA 18974		13. NUMBER OF PAGES 64	
		15. SECURITY CLASS. (of this report) Unclassified 12/62p.	
16. DISTRIBUTION STATEMENT (of this Report) "Approved For Public Release - Distribution Unlimited"		15a. DECLASSIFICATION/DOWNGRADING SCHEDULE	17. R02204001
17. DISTRIBUTION STATEMENT (of the abstract entered in Block 20, if different from Report)			
18. SUPPLEMENTARY NOTES			
19. KEY WORDS (Continue on reverse side if necessary and identify by block number) Ceramics for Gas Turbine Engines Silicon Nitride Composites Tantalum Reinforced Silicon Nitride High Impact Strength Ceramics			
20. ABSTRACT (Continue on reverse side if necessary and identify by block number) Tantalum wire reinforced hot-pressed Si_3N_4 offers a significant improvement in Charpy and ballistic impact strength from RT to 1300°C over monolithic hot-pressed Si_3N_4 . The elastic modulus of $Si_3N_4 + 15\% Y_2O_3$ reinforced with 25 vol %, 25 mil Ta wires as measured by an ultrasonic pulse echo test is 41.5×10^6 psi (287 GPa) at RT, falling to 38.7×10^6 psi (267 GPa) at 1050°C. The thermal expansion coefficient of $Si_3N_4 + 15$ wt % Y_2O_3 hot-pressed material was			

20. Continued

measured as $2.9 \times 10^{-6}/^{\circ}\text{C}$ from RT to 925°C and $3.4 \times 10^{-6}/^{\circ}\text{C}$ from RT to 1300°C . The corresponding values for this matrix reinforced with 25 vol % Ta wires are $3.2 \times 10^{-6}/^{\circ}\text{C}$ and $3.8 \times 10^{-6}/^{\circ}\text{C}$. The thermal conductivity of a Si_3N_4 + 20 vol %, 25 mil Ta composite in the direction parallel to the Ta wires was measured as $47 \text{ Wm}^{-1} \text{ K}^{-1}$ at 50°C , falling gradually to $22 \text{ Wm}^{-1} \text{ K}^{-1}$ at 1000°C . These values are 42% and 16% higher, respectively, than the thermal conductivity measured for monolithic hot-pressed Si_3N_4 . The critical stress intensity factor (K_{IC}), measured from the notched beam test, of Si_3N_4 + 15% Y_2O_3 reinforced with Ta wires was $8.6 \text{ MN/m}^{3/2}$ at RT and $5.3 \text{ MN/m}^{3/2}$ at 1300°C . The RT value represents a 25% increase over comparable monolithic Si_3N_4 material.

UNITED TECHNOLOGIES RESEARCH CENTER



East Hartford, Connecticut 06108

Report R77-912538-4

Evaluation of Tantalum Fiber
Reinforced Si_3N_4

REPORTED BY

J. J. Brennan
J. J. Brennan

APPROVED BY

E. R. Thompson
E. R. Thompson, Manager
Materials Sciences

ACCESSION for	
RTIS	White Section <input checked="" type="checkbox"/>
DDC	Buff Section <input type="checkbox"/>
UNANNOUNCED	<input type="checkbox"/>
JUSTIFICATION	
BY	
DISTRIBUTION/AVAILABILITY CODES	
DIST.	AVAIL. RES. OR SPECIAL
A	

Evaluation of Tantalum Fiber Reinforced Si₃N₄

TABLE OF CONTENTS

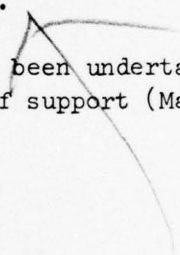
I.	INTRODUCTION	1
II.	SUMMARY OF PREVIOUS WORK	2
III.	Si ₃ N ₄ -Ta DESIGN PROPERTY VALUES	5
	3.1 Elastic Modulus	5
	3.2 Thermal Expansion Coefficient	6
	3.3 Thermal Conductivity	6
	3.4 Shear Strength	8
	3.5 Tensile Strength	9
IV.	Si ₃ N ₄ -Ta FRACTURE MECHANICS TESTS	11
	4.1 Notched Beam Tests	12
	4.2 Double Torsion Tests	16
V.	CONCLUSIONS	19
VI.	ACKNOWLEDGEMENTS	21
	REFERENCES	22
	TABLES I - VI	24
	FIGURES 1 - 28	
	APPENDIX	



I. INTRODUCTION

Ceramic materials, by virtue of their high melting points and oxidation resistance, can offer large gains in gas turbine performance, provided some serious limitations can be overcome. These are poor thermal shock resistance and, more critically, low impact strength. Hot-pressed silicon nitride, currently the leading candidate for use as a high temperature vane material, has not only good oxidation resistance but also very good thermal shock resistance for a ceramic material. However, its use is still limited by its relatively low impact strength. It is the solution of this problem that UTRC has emphasized in the current contract with NADC on improving the impact strength of Si_3N_4 through the use of fiber or wire reinforcements. This approach provides energy absorption modes not available in monolithic materials. By tailoring the properties of the composite it is possible not only to maximize energy absorption during impact but to control the type of fracture as well. Small fragments breaking out of vanes are probably tolerable under abnormal impact loads whereas total failure is unacceptable.

This report summarizes the research activity which has been undertaken by United Technologies Research Center during the fifth year of support (March 1, 1976 - March 1, 1977) under Contract N62269-76-C-0104.



II. SUMMARY OF PREVIOUS WORK

During the first year of work (January 1972 - January 1973) on the subject of fiber reinforced Si_3N_4 under NASC contract N00019-72-C-0377, it was found that tungsten reinforced hot-pressed Si_3N_4 results in up to a ninefold increase in the elevated temperature (1300°C) Charpy impact strength over monolithic Si_3N_4 , primarily due to the energy absorbing mechanism of fiber pullout. However, the RT Charpy impact strength of Si_3N_4 -W composites is not increased over that of unreinforced Si_3N_4 due to the brittle nature of the silicide reaction product which forms at the Si_3N_4 -W interface and the notch sensitivity of tungsten. Attempts were made to stop the formation of this silicide layer either by lowering the fabrication temperature or by applying a reaction barrier coating on the tungsten wires. These attempts met with only limited success.

Near the end of the first year's program it was found that tantalum wire reinforced Si_3N_4 increased the RT Charpy impact strength by a factor of 30 (0.5 ft-lbs to 14.8 ft-lbs) and also affected the mode of failure such that interfacial splitting along with ductile fiber elongation occurred, resulting in very small fragments of matrix breaking off upon impact. A ceramic part exhibiting this mode of fracture is desirable for possible use in gas turbine engines.

During the second year of work (March 1973 - March 1974) on the subject of fiber reinforced Si_3N_4 under NADC contract N62269-73-C-0268, hot-pressed Si_3N_4 containing 25 volume percent of 25 or 50 mil tantalum wires was found to increase the Charpy impact strength of Si_3N_4 by a factor of over 30 (from 0.5 ft-lbs to 16 ft-lbs) at temperatures from RT to 1300°C. Hot pressing was done at 1675°C for 30 min in Ar. The mode of failure is also affected such that interfacial splitting along with ductile wire elongation occurs, resulting in very small fragments of matrix breaking off upon impact, in contrast to large pieces resulting from an unreinforced Si_3N_4 failure.

The Ta- Si_3N_4 composite system has also been found to exhibit a threshold energy below which no damage occurs upon impact that is considerably higher than unreinforced Si_3N_4 . This energy has been found to be from 2-3 ft-lbs for a Charpy sized composite specimen compared to 0.5 ft-lbs for unreinforced Si_3N_4 . This effect has been observed in instrumented and low energy Charpy impact at RT and in ballistic impact at both RT and 1300°C.

A thermal fatigue test that allowed samples to be heated from 200°C to 1300°C in one minute using a propane-oxygen torch and then cooled to 200°C in one and a half minutes using a cold air blast showed that no significant degradation of impact properties occurred for up to 100 cycles. Also, the mechanisms of failure of the composite were not affected. In addition, thermal aging in air at 1300°C for up to 1000 hrs did not significantly lower the Si_3N_4 -Ta composite impact strength nor affect the mechanisms of failure.

From the third year's work on this subject (March 1974 - March 1975), it was found that using from 10-15 weight percent Y_2O_3 as the densification aid for hot-pressing Si_3N_4 instead of the standard 5 weight percent MgO increased the average modulus of rupture for the matrix from 120 ksi to 140 ksi at RT and from 40 ksi to 73 ksi at 1300°C. Likewise, the Si_3N_4 -Ta composite MOR was increased from 80 ksi to over 100 ksi at RT and from 35 ksi to 51 ksi at 1300°C.

It was also found that the 1300°C 15,000 psi creep rate for $Si_3N_4 + 10\% Y_2O_3$ material is an order of magnitude less than the $Si_3N_4 + 5\% MgO$ material, with Ta reinforced $Si_3N_4 + 10\% Y_2O_3$ performing as well, or even better than the unreinforced sample.

In addition, considerable effort was devoted to the "pseudo-isostatic" hot-pressing method to fabricate airfoil shapes from Si_3N_4 and Si_3N_4 -Ta composites. Briefly, this method consists of cold isostatic pressing a shape out of Si_3N_4 powder, with appropriate additive, and then surrounding this shape in a medium of BN powder inside a graphite hot-press die. The BN acts as a powder vehicle that transfers pressure to the preformed piece. Using a hot-pressing schedule of 7 MN/m² (1000 psi) at 1630°C, 13.8 MN/m² (2000 psi) at 1700°C, and 21 MN/m² (3000 psi) at 1750°C, with a 30 min hold at the final temperature, shapes of over 99 percent theoretical density have been made from $Si_3N_4 + 10\% Y_2O_3$, both with and without Ta wire reinforcement.

From the fourth year's work on this subject, it was found that silicide coatings on the Ta wires can successfully prevent oxidation attack of the wires at elevated temperatures in air, but when incorporated into a hot-pressed Si_3N_4 matrix, the presilicided wires offer little improvement over uncoated wires when exposed to air due to matrix fracture. Also, the presilicided Ta- Si_3N_4 composites are generally inferior in impact resistance due to the thicker total silicide layer at the Ta- Si_3N_4 interface.

Other findings from the fourth year's work are:

- The matrix material $Si_3N_4 + 15 \text{ wt } \% Y_2O_3$ (low Ca content Si_3N_4) is superior in strength at both RT and 1300°C to any other Si_3N_4 - Y_2O_3 combination tested and the previously used $Si_3N_4 + 5\% MgO$ material. This matrix in combination with 25 vol % Ta wires also results in superior RT and 1300°C MOR values over previously tested composites. The Weibull modulus (m) of $Si_3N_4 + 15\% Y_2O_3$ -Ta composites tested at RT in 3-pt bending is 5.1. The average strength of these composite samples is 99.6 ksi.
- The strength of hot-pressed $Si_3N_4 + 15 \text{ wt } \% Y_2O_3$ is severely degraded at intermediate temperatures of 800-1000°C when the starting powder consisted of AME α - Si_3N_4 with high Ca, Fe, and Al impurities but was not degraded when the starting powder was low in Ca, Fe, and Al impurities.

- The high temperature ($\Delta T = 1260^{\circ}\text{C}$) thermal fatigue of $\text{Si}_3\text{N}_4 + 10\text{-}15$ wt % Y_2O_3 , both with and without 25 vol %, 25 mil Ta wire reinforcement, appears to be comparable to Norton NC-132 Si_3N_4 ; however, thermal fatigue wedges containing 25 vol %, 50 mil Ta wires appear to fail prematurely due to fracture of the matrix material caused by stresses generated at the Si_3N_4 -Ta wire interface from thermal expansion differences between the Si_3N_4 and Ta.
- The high temperature (1300°C) creep of Ca free $\text{Si}_3\text{N}_4 + 15\%$ $\text{Y}_2\text{O}_3 + 25$ vol % Ta was measured in bending at an applied stress of 15,000 psi. The resultant steady state creep rate of $1.5 \times 10^{-6}/\text{hr}$ was more than an order of magnitude less than that for high Ca $\text{Si}_3\text{N}_4 + 10\%$ $\text{Y}_2\text{O}_3 + 25$ vol % Ta and three orders of magnitude less than high Ca $\text{Si}_3\text{N}_4 + 5\%$ $\text{MgO} + 25$ vol % Ta. It was also substantially less than that for commercially available hot-pressed Si_3N_4 .

During the past year's work on this contract, study was directed toward the fracture mechanics of the Si_3N_4 -Ta system and the determination of design property values such as thermal expansion coefficient, thermal conductivity, elastic modulus, and shear strength. Critical stress intensity factors (K_{IC}) of both Ta reinforced and unreinforced Si_3N_4 were determined at RT and 1300°C through the use of the notched beam test. In addition, crack growth rates were measured at RT and 1300°C using the double torsion test and the ultimate tensile strength was measured, also at RT and 1300°C .

III. Si_3N_4 -Ta DESIGN PROPERTY VALUES

3.1 Elastic Modulus

The elastic (Young's) modulus of $\text{Si}_3\text{N}_4 + 15\% \text{Y}_2\text{O}_3$ reinforced with 25 vol %, 25 mil Ta wires was measured in 4-point bending at RT. The resultant value of 44.5×10^6 psi (307 GPa) compares quite well with values normally found for commercial hot-pressed Si_3N_4 (45×10^6 psi) (Ref. 1). From the rule of mixtures, one could expect the modulus of the Si_3N_4 -Ta composite to be approximately 41×10^6 psi. The reason that the measured value is higher is probably due to the fact that 40 mils of Si_3N_4 separated the tensile surface of the sample from the first layer of Ta wires with the wires being located towards the low stress center area of the sample. Therefore, this test was performed on another Si_3N_4 -Ta sample with the Ta wires only 15 mils from the tensile surface. The results of this test gave a modulus value of 36.7×10^6 psi (253 GPa). Therefore, the distance from the tensile surface of the Ta wires does affect the elastic modulus of the composite as measured in bending.

Since strain gages are capable of operation to temperatures of only 400°C or so, the measurement of elastic modulus at higher temperatures must be done using another method than that used at RT. UTRC has recently put into operation a dynamic modulus measuring system that is capable of measurements to 1100°C . The elastic modulus of a material may be measured using high frequency sound pulses through the relation:

$$E = \rho v^2; \quad \rho = \text{density} \\ v = \text{speed of sound.}$$

The UTRC facility employs two instruments manufactured by Panametrics, Inc. which generate ultrasonic pulses and measure the time required for the pulse to traverse a fixed length of material.

By suitably mounting a specimen of material whose modulus is to be measured, echoes from a known length of material can be selected and the corresponding traverse time of the ultrasonic pulse can be measured. If a sufficient length of material is available, a properly prepared specimen can be made to yield echoes from a length within the sample, so that phase corrections at the mounting joint are not required.

Measurements of modulus vs temperature can be carried out once the specimen has been prepared and mounted using a furnace with various gaseous atmospheres. Shear modulus as well as tensile modulus can be obtained using the appropriate ultrasonic transducer.

Figures 1 and 2 show the oscilloscope traces of an ultrasonic pulse as it echoes back from a known length of monolithic Si_3N_4 (Norton NC-132) and $\text{Si}_3\text{N}_4 + 15\% \text{Y}_2\text{O}_3 + 25 \text{ vol } \% \text{Ta}$, respectively, measured at RT. By measuring the distance between peaks, i.e. the time between echoes, the elastic modulus of the two materials was calculated as 45.7×10^6 psi (315 GPa) for the NC-132 and 41.5×10^6 psi (287 GPa) for the Si_3N_4 -Ta composite. These values are in good agreement with measurements done previously in 4-pt bending.

The same samples were then tested to over 1000°C with the results shown in Fig. 3. Modulus values for monolithic NC-132 Si_3N_4 of 43.9×10^6 psi (303 GPa) and 40.9×10^6 psi (282 GPa) were recorded at 500°C and 1000°C respectively. The Ta reinforced Si_3N_4 sample exhibited moduli of 39.9×10^6 psi (275 GPa) and 38.7×10^6 psi (267 GPa) at the same two temperatures. From these results it is apparent that Ta reinforced Si_3N_4 exhibits a lower elastic modulus than monolithic Si_3N_4 at all temperatures from RT to 1100°C with the difference between the two materials narrowing as the temperature increases.

3.2 Thermal Expansion Coefficient

The thermal expansion coefficient of $\text{Si}_3\text{N}_4 + 15 \text{ wt } \% \text{Y}_2\text{O}_3$, both with and without Ta wire reinforcement, was measured twice; initially from RT to 925°C and then from RT to 1300°C when a higher temperature Theta dilatometer rig became available. The results of these tests are shown in Figs. 4 and 5 and in Table I. The average value of coefficient of thermal expansion for the $\text{Si}_3\text{N}_4 + 15\% \text{Y}_2\text{O}_3$ material was found to be $2.9 \times 10^{-6}/^\circ\text{C}$ from RT to 925°C and $3.4 \times 10^{-6}/^\circ\text{C}$ from RT to 1300°C . Literature values are comparable, with Gazza (Ref. 2) obtaining $3.37 \times 10^{-6}/^\circ\text{C}$ (RT to 1000°C) for 10 wt % Y_2O_3 material and Tsuge, et al (Ref. 3) reporting a value of $3.5 \times 10^{-6}/^\circ\text{C}$ (RT to 1200°C) for 5 wt % Y_2O_3 material.

The average coefficient of thermal expansion for the $\text{Si}_3\text{N}_4 + 15\% \text{Y}_2\text{O}_3 - 25 \text{ vol } \% \text{Ta}$ composite was found to be $3.2 \times 10^{-6}/^\circ\text{C}$ (RT \rightarrow 925°C) and $3.8 \times 10^{-6}/^\circ\text{C}$ (RT \rightarrow 1300°C), slightly higher than the monolithic material but less than that calculated from rule of mixtures ($4.0 \times 10^{-6}/^\circ\text{C}$, RT \rightarrow 1000°C). The tantalum wires apparently do increase the thermal expansion of the Si_3N_4 matrix somewhat.

3.3 Thermal Conductivity

The thermal conductivity in the direction parallel to the Ta wires in a Si_3N_4 -Ta composite was measured at Dynatech R/D Co., Cambridge, MA. The conductivity was measured at six temperatures; 40°C , 200°C , 400°C , 600°C , 800°C , and 1000°C , using the axial rod method. This method consists of supplying a

carefully measured, constant heat input to one end of a long cylindrical or rectangular cross-section sample, while the opposite end is placed in contact with a heat sink. Thus, a heat flux is established through the sample, creating an axial temperature gradient. The size of the temperature gradient depends on the thermal conductivity of the specimen. Temperatures are measured along the length at calibrated intervals.

The sample conductivity is determined from the Fourier heat flow equation as follows:

$$\lambda = \frac{q/A}{dT/dx}$$

where λ = local thermal conductivity, watt/cm °C
 q = heat input to the sample heater, watt
 A = sample cross-sectional area, cm²
 dT/dx = local temperature gradient in the test sample as determined from a number of axial temperature measurements, °C/cm.

It is obvious that the instantaneous conductivity versus temperature relationship may be obtained over the entire range between the highest and the lowest sample temperatures. The above procedure is valid as long as all measured heat input does indeed pass through the rod in the direction of the heat sink without losses or gains along the way.

The Si₃N₄-Ta sample that was fabricated for use in this measurement had dimensions of 0.5 in. x 0.5 in. x 2.25 in. with thermocouple slots 0.030 in. wide by 0.040 in. deep diamond sawed along one side of the sample at 0.25 in. intervals. The bottom of the thermocouple slots was within 0.010 in. of the first layer of Ta wires. There were ten layers of Ta wires in the sample at ten wires per layer for a total of 100 wires.

The results of the conductivity measurements, compared to published values for Norton Co. NC-132 Si₃N₄, are shown in Fig. 6. As can be seen from Fig. 6, the thermal conductivity of the Si₃N₄-Ta composite is greater than that of monolithic Si₃N₄, as expected; being 42% higher at RT and dropping to 16% higher at 1000°C.

The measured conductivity values for Si₃N₄-Ta and NC-132 are shown also in Table II, along with the calculated values in both the longitudinal and transverse directions for Si₃N₄-Ta using the equations given by Ashton, et al (Ref. 4). Ashton's equation for the longitudinal direction is simply the rule of mixtures equation:

$$K_{\text{Long.}} = V_f K_f + V_m K_m$$

where V_f , K_f , V_m , and K_m are the volume fraction and thermal conductivity of the fibers and matrix, respectively. The particular composite sample used was found to contain only 20 vol % Ta wires, as opposed to the usual 25 vol %.

It can be seen that the calculated values do not correspond particularly well with the measured values except at intermediate temperatures, being too low at low temperatures and too high at the higher temperatures. Part of the problem could be due to the extreme scatter in data for the thermal conductivity of tantalum as a function of temperature. From the data given in "Thermophysical Properties of High Temperature Solid Materials" (Ref. 5) it was found that, depending on the source, values of the RT thermal conductivity of tantalum vary from 0.10 to 0.34 Btu hr⁻¹ ft⁻¹ R⁻¹ x 10² (17.3 to 58.8 Wm⁻¹ K⁻¹) and at 1000°C vary from 0.29 to 0.43 Btu hr⁻¹ ft⁻¹ R⁻¹ x 10² (50.2 to 74.3 Wm⁻¹ K⁻¹). It was decided to assume that the conductivity of tantalum is constant with temperature, as many of the data points appear to indicate, and the value of 0.34 Btu hr⁻¹ ft⁻¹ R⁻¹ x 10² (58.8 Wm⁻¹ K⁻¹) as found by Tye (Ref. 6) was chosen for the calculations, in part because Tye performed the measurements at Dynatech on the Si₃N₄-Ta material.

Although the measured and calculated values of the longitudinal thermal conductivity do not agree precisely, the transverse thermal conductivity was calculated for the Si₃N₄-Ta composite using Ashton's equation:

$$K_{\text{trans.}} = K_m (1 + \zeta \eta V_f) / (1 - \eta V_f)$$

where $\eta = (K_f/K_m - 1) / (K_f/K_m + \zeta)$ and $\log \zeta = \sqrt{3} \log(a/b)$, a and b being the width and thickness of the reinforcing media, in this case since the Ta wires are circular in cross-section $a = b$ and thus $\zeta = 1$. The calculated values are given in Table II and, if accurate, indicate that the transverse thermal conductivity at all temperatures from 50°C to 1000°C is higher than the longitudinal thermal conductivity. Thus the observation can be made that the thermal conductivity of Ta reinforced Si₃N₄ is substantially higher than that of monolithic Si₃N₄ and thus the thermal shock properties of the composite should be somewhat better than that of the Si₃N₄ matrix alone, as water quench tests done previously have indicated.

3.4 Shear Strength

Short beam shear strength measurements were done at RT and 1300°C on Si₃N₄-Ta composite samples, the results of which are given in Table III. Of the six samples tested at RT and three tested at 1300°C, none actually failed in pure shear. Two RT samples and one 1300°C sample exhibited some shear component in

their failure mode but primary failure was due to tensile stresses on the lower surface of the bend specimens. The average bend stresses to cause failure at RT were 130 ksi (895 MPa) and at 1300°C were 45 ksi (310 MPa).

One of the samples that failed in bending at RT but exhibited some shear component is shown in Figs. 7 and 8. The sample was treated with Zyglo dye penetrant and photographed under ultraviolet light so that the crack pattern would be readily visible. From these figures it can be seen that the crack origin occurred on the tensile face but that as the crosshead motion increased the sample began shearing along the Ta wire-Si₃N₄ interfaces such that longitudinal cracks were formed in the plane of the Ta wires. One sample was tested at RT in a fixture that applied a compressive shear load parallel to the Ta wires. This sample withstood a shear stress of 15.5 ksi (107 MPa) before the loading ram sheared off.

Since the samples did not fail primarily in shear, the listed shear values in Table III are not particularly meaningful. It is somewhat surprising that shear failure did not occur in this system since, from impact results, it is obvious that the Si₃N₄-Ta interfacial bond is quite weak. Evidently the fairly large fiber-to-fiber distance and the high strength of the Si₃N₄ matrix material inhibits shear failure from occurring.

3.5 Tensile Strength

The uniaxial tensile strength of Si₃N₄ + 15% Y₂O₃ material was measured at RT and 1300°C. The UTS of Si₃N₄-Ta was measured at RT. The configuration of the tensile test samples is shown in Fig. 9. The samples were 2 1/2 in. long with a minimum cross-section of 0.100 in. x 0.100 in. at the narrowest point. The finish grind of the reduced section was done with a 320 grit diamond wheel with all grinding marks parallel to the tensile direction. The sharp corners of the reduced section were slightly rounded by hand using 600 grit SiC paper. The tensile test procedure is outlined in greater detail in the Appendix.

The results of these tests are given in Table IV. The two Si₃N₄ + 15% Y₂O₃ samples tested at RT (UTS-1,2) both failed slightly away from the minimum cross-sectional point with fracture initiating at internal flaws. Figures 10, 11 and 12 are scanning electron micrographs of the fracture surface of sample UTS-2 and show clearly the origin of fracture, which appears to be an area of low density (void) fairly close to one side of the sample. The UTS of this sample at the point of fracture of 83.6 ksi (577 MPa) is as high or higher than any previously recorded by other researchers for hot-pressed Si₃N₄. Richardson (Ref. 7) recorded a value of 79.6 ksi at RT for Norton NC-132, while Pratt and

Whitney (Ref. 8) and Westinghouse (Ref. 9) found average RT UTS values of approximately 55 ksi for earlier Norton material, HS-130. The observation that both samples UTS-1 and 2 failed at internal voids is significant in that the fabrication of void-free material should result in higher UTS values than those observed in this study. The internal failures also indicate that a true tensile stress was applied on the sample during testing.

The RT UTS of a $\text{Si}_3\text{N}_4 + 15\% \text{Y}_2\text{O}_3$ sample reinforced with 25 mil Ta wires was a disappointingly low 24.0 ksi (166 MPa). Figures 13 and 14 are scanning electron micrographs of the fracture surface and, although it is not unequivocally obvious, appear to indicate that the failure initiated at the interface between one of the four Ta wires and the Si_3N_4 matrix. Thus in pure tension, where the stresses are evenly distributed throughout the cross section of the sample, the large diameter Ta wires are acting as massive flaws and concentrating stresses at their surfaces. In bending, where the maximum stress is on the surface of the sample, with the internal Ta wires being subjected to much lower stresses, much less reduction in strength is observed due to the Ta wires. Therefore, the use of Ta reinforced Si_3N_4 as a structural ceramic in gas turbine engines appears to be limited to nonrotating components such as vanes.

The Ta reinforced sample (UTS-5) scheduled for 1300°C tensile testing was inadvertently fractured prior to testing. Thus, no data were generated concerning the elevated temperature tensile strength of Si_3N_4 -Ta composite material. The unreinforced $\text{Si}_3\text{N}_4 + 15\% \text{Y}_2\text{O}_3$ sample UTS-3 was tested in tension at 1300°C, however, with a tensile strength of 61 ksi (420 MPa) being recorded. The fracture origin of this sample, as was the case at RT, was at an internal flaw. The value of 61 ksi recorded for the Si_3N_4 - Y_2O_3 material at 1300°C is over twice as high as that recorded for HS-130 Si_3N_4 at 1300°C of 29.1 ksi by Pratt and Whitney (Ref. 8). This is another demonstration of the superior high temperature strength capability of Y_2O_3 additive hot-pressed Si_3N_4 over the conventional MgO additive material.

IV. Si_3N_4 -Ta FRACTURE MECHANICS TESTS

Fracture mechanics design criteria recognizes that the presence of either cracks or crack initiators (inclusions) can cause ceramics to fail at much lower stresses than expected from stress levels established from average bulk tensile or flexural tests. The fracture mechanics approach deals with two fundamental considerations; (1) the critical crack length before failure and (2) the number of cycles required for the crack to reach this critical size. To determine this information, one must solve the basic equation:

$$\frac{da}{dn} = AK^B$$

where: a = crack length
n = number of cycles
K = stress intensity factor
A,B = experimentally determined constants.

The basic parameter used in fracture mechanics is K, the stress intensity factor. For an infinite plate containing a crack of length a and a stress σ ; $K = \sigma\sqrt{\pi a}$. All other geometries use this basic equation with a correction constant C to account for width, crack shape and location. Thus, $K = \sigma C\sqrt{\pi a}$. For any component or test specimen there is some combination of stress and crack size which causes the crack to become unstable and grow rapidly to failure. For a static part with a fixed crack size, failure occurs if the load is increased to a critical value. For a part with cyclic loading, the crack can grow slowly with each cycle until it reaches critical size and fails, or it can grow rapidly such that the threshold intensity factor K_{TH} , where initial crack propagation is first observed, and the critical intensity factor K_C at failure, are virtually equal. If the stress, crack length and proper correction factors are used to calculate the stress intensity factor at failure, it will be a constant for a given material and temperature. This value is called the critical stress intensity factor, K_{IC} , or the fracture toughness of the material. If the fracture toughness and operating stress are known for a component design, the critical crack size can be estimated. If the rate at which a crack grows from initial size to critical size is known, then the component life can be determined.

In the case of Ta reinforced Si_3N_4 it would be desirable to know whether or not K_{IC} and the rate of crack growth are affected by the presence of the wires. Lange (Ref. 10) has found that for monolithic hot pressed Si_3N_4 subcritical crack growth is responsible for high temperature strength degradation and that calculated K_{IC} values at elevated temperature are approximately twice those reported for RT. Wiederhorn (Ref. 11) has also identified subcritical crack growth in hot-pressed Si_3N_4 at temperatures as high as 1400°C and higher K_{IC} values as the temperature is increased.

4.1 Notched Beam Tests

The fracture mechanics test specimen used to determine K_{IC} values is the notched beam specimen shown in Fig. 15. This test was selected to provide a measurement of K_{IC} values due to the much greater ease of sample preparation over that necessary for somewhat more accurate methods such as the double cantilever beam. Despite questions of the absolute accuracy of the method, the NBT is believed to provide a good relative ranking of materials (Ref. 12). A 6 mil thick diamond saw was used to form the slot in the specimen. Loading rates were 0.0025 in./min.

The value of the critical stress intensity factor (K_{IC}) was calculated from the following equation (Refs. 13,14):

$$K_{IC} = \frac{3 P \ell \sqrt{c}}{2bd^2} \left[A_0 + A_1 \left(\frac{c}{d} \right) + A_2 \left(\frac{c}{d} \right)^2 + A_3 \left(\frac{c}{d} \right)^3 + A_4 \left(\frac{c}{d} \right)^4 \right]$$

where P = failure load

ℓ, b, d & c are specimen dimensions shown in Fig. 15

$$A_0 = 1.90 + 0.0075X$$

$$A_1 = -3.39 + 0.08X$$

$$A_2 = 15.40 - 0.2175X$$

$$A_3 = -26.24 + 0.281X$$

$$A_4 = 26.28 - 0.145X$$

$$X = d/b$$

This equation is valid for $c/d \leq 0.6$ and has been found to give somewhat higher values for the K_{IC} of ceramic materials as the c/d ratio decreases (Ref. 15).

Twelve samples of Si_3N_4 , both with and without Ta wire reinforcement, were tested in the notched beam configuration at RT. The results are given in Table V. The first sample (KC-1), with a rather low c/d of 0.25 and a 25 mil distance between the saw cut and the first layer of Ta wires, gave a K_{IC} value of $13.95 \text{ MN/m}^{3/2}$. The fracture surface of this sample is shown in Fig. 16. All samples containing Ta wires had to be physically broken after test since complete fracture did not occur during the notched beam testing. A Si_3N_4 -Ta sample (KC-2) was also tested with the saw cut extending about 10 mils into the first layer of Ta wires (i.e., about halfway through the Ta wire). The c/d ratio of this sample was slightly higher (0.31) while its measured K_{IC} value was much lower ($3.85 \text{ MN/m}^{3/2}$). The fracture surface of this sample is shown in Fig. 17. Whereas the first Si_3N_4 -Ta sample (KC-1) exhibited a linear stress-strain curve up to the point of fracture, sample KC-2 exhibited an essentially plastic stress-strain curve indicating that the Ta wires were deforming on initial application of load. Wire-to-wire cracking of the matrix was undoubtedly occurring continuously as loading continued.

The next two samples tested (KC-3 and KC-4) contained no Ta wire reinforcement, one with a c/d ratio of 0.25 (identical to KC-1) and another with a deeper notch with a c/d of 0.60. Sample KC-3, with c/d of 0.25, exhibited a K_{IC} of $6.55 \text{ MN/m}^{3/2}$ while KC-4 (c/d = 0.60) had a K_{IC} of $5.03 \text{ MN/m}^{3/2}$. These data substantiate the observation by others that K_{IC} decreases with increasing c/d ratio (Ref. 15). The large difference in K_{IC} between sample KC-1 with Ta wires ($13.95 \text{ MN/m}^{3/2}$) and KC-3 without Ta wires ($6.55 \text{ MN/m}^{3/2}$) suggests that the presence of the Ta wires at a distance from the notch increases the fracture toughness of the material. Both samples KC-3 and KC-4 appeared to contain areas that were not quite fully dense, which could lead to lower strength and K_{IC} values. Literature values for K_{IC} of hot-pressed Si_3N_4 measured by the notched beam test tend to fall between 3.4 and $6.8 \text{ MN/m}^{3/2}$ at RT (Refs. 12,16).

From the results of samples KC-1 to KC-4, it was decided to standardize the notch depth to sample thickness ratio (c/d) at 0.50 and to try to obtain as near theoretical density as possible in the $\text{Si}_3\text{N}_4 + 15\% \text{ Y}_2\text{O}_3$ matrix material. Samples KC-6 through KC-8 were hot-pressed at temperatures from 1725°C to 1775°C and were found to be essentially fully dense at only the higher temperature of 1775°C . The increase in K_{IC} as the density increases is significant. While samples KC-8 and KC-9 are both essentially fully dense, KC-9 exhibits a higher K_{IC} value, apparently due to the increased time of hot pressing (1 hr for KC-9, 30 min for KC-8). It has been proposed by Messier, et al (Ref. 17) and Iskoe, et al (Ref. 18) that the excellent mechanical properties of hot-pressed Si_3N_4 are due to the $\alpha \rightarrow \beta$ transformation during hot-pressing that results in an elongated grain structure. However, densification can occur without complete $\alpha \rightarrow \beta$ transformation occurring. It was thought, therefore, that sample KC-8, while fully dense, might not be completely transformed to $\beta\text{-Si}_3\text{N}_4$ while KC-9 was transformed and thus exhibited a higher K_{IC} value. X-ray analysis of these samples, however, showed only $\beta\text{-Si}_3\text{N}_4$ peaks for both samples. It is interesting to note that Norton NC-132 Si_3N_4 exhibits a substantially lower K_{IC} value ($4.71 \text{ MN/m}^{3/2}$) than the $\text{Si}_3\text{N}_4 + 15\% \text{ Y}_2\text{O}_3$ material (KC-9, $6.75 \text{ MN/m}^{3/2}$). This has been observed by others (Ref. 19) and apparently is related to the different grain boundary phases present in MgO additive Si_3N_4 (NC-132) as compared to Y_2O_3 additive Si_3N_4 . MgO additive Si_3N_4 can have glassy phases present at the grain boundaries, whereas Y_2O_3 additive Si_3N_4 generally contains crystalline grain boundary phases.

Samples KC-10 and KC-11, which contained Ta wire reinforcement, exhibited significantly higher K_{IC} values than the corresponding monolithic Si_3N_4 matrix material. As with the unreinforced samples, hot-pressing for 1 hr at 1775°C gave higher K_{IC} values than a 30 min hot-press. The K_{IC} value for the composite sample KC-11 of $8.57 \text{ MN/m}^{3/2}$ is over 25% higher than that for the monolithic sample KC-9 of $6.75 \text{ MN/m}^{3/2}$. In sample KC-11, the Ta wires were only 3 mils away from the tip of the notch. The difference in behavior during testing of samples KC-9 and KC-11 is indicated in Fig. 18 which shows the stress-midspan

deflection curves for both samples. The point of initial notch extension for KC-11 is noted and it is this load that was used to compute the K_{IC} value. It can be seen that as the load is increased beyond this point additional crack movement and branching is occurring as the crack jumps from wire to wire and moves along the Ta wire-Si₃N₄ interfaces. After testing to a total load of almost twice the load for initial crack propagation and a midspan deflection of over 0.02 in., both samples KC-10 and KC-11 appeared to be uncracked when the load was released. Only upon Zyglo dye penetrant inspection can the crack extension be seen, as shown in Fig. 19. A significant amount of crack branching is occurring parallel to the Ta wires.

The distance from the notch tip to the Ta wires is shown in Figs. 20 and 21 for samples KC-10 and KC-11, respectively, after the samples had been fractured completely through. The notch tip is about 10 mils from the Ta wires in KC-10 and only about 3 mils from the first 25 mil diameter Ta wire in KC-11. From the results to date, it appears that the extension of a crack in the matrix of a Si₃N₄-Ta composite may be more difficult than in the monolithic Si₃N₄ material, even when the crack is very close to a Ta wire.

Seven samples of Si₃N₄, both with and without Ta wire reinforcement, were tested in the notched beam configuration at 1300°C. The results are shown in Table VI. Two of the samples, KC-12 and KC-14, were unfortunately destroyed before any meaningful data could be obtained from them. Sample KC-12 broke when thermal expansion of the alumina rams during heat-up caused the loading nose, which was initially set too close to the sample, to contact the sample and fracture it. The recorder that monitors the load applied to the sample during test was not turned on yet and thus the fracture of the sample went unnoticed. Sample KC-14 was destroyed when the ceramic block under the 3-pt bend fixture melted at the test temperature of 1300°C. This block was originally thought to be alumina but obviously was not.

The two samples without Ta wires that were successfully tested at 1300°C, KC-15 and 16, exhibited quite different critical stress intensity factors, 8.00 and 5.30 MN/m^{3/2}, respectively. These values bracket the RT value for a fully dense specimen of 6.75 MN/m^{3/2}. The fracture surfaces of both specimens appeared very similar with the only differences between samples being a slight density variation; KC-15 being 3.36 gms/cc while KC-16 being slightly lower at 3.34 gms/cc. It is possible that the slightly lower density of KC-16 could be responsible for its lower K_{IC} value. The high value of 8.00 MN/m^{3/2} is somewhat surprising since no evidence of plastic deformation due to a glassy grain boundary phase was noted, with the stress strain curve of sample KC-15 being very linear (as was KC-16). This curve, as well as that for a sample with Ta wires (KC-13) is shown in Fig. 22. An increase in K_{IC} for Si₃N₄ densified with MgO at elevated temperatures has been found by other researchers (Refs. 16,20)

and has been attributed to the presence of a grain boundary glassy phase that becomes soft at high temperatures leading to crack blunting. Silicon nitride densified with 15 w/o Y_2O_3 should not contain any glassy phase and thus would not be expected to exhibit an increase in K_{IC} at elevated temperatures.

Samples KC-13, 17, and 18, which contained Ta wire reinforcement, all exhibited lower K_{IC} values (5.36, 4.70 and 5.06 $MN/m^{3/2}$, respectively) than similar samples tested at RT (7.88 and 8.57 $MN/m^{3/2}$). From Fig. 22 it is apparent that after the initial crack extension at the point of maximum load, the wires do not add significantly to the residual strength of the composite. This is in contrast to the great amount of load carrying ability and crack deflection and branching that occurs at RT, as shown in Fig. 18. Figure 23 shows the fracture surface of sample KC-13. Comparing this to the fracture surface of sample KC-10 (Fig. 20) tested at RT, it is apparent that the 1300°C fracture surface of KC-13 is much smoother than KC-10 and that there is no significant crack deflection due to the Ta wires. It is quite possible that at RT a significant amount of residual compressive stress is present in the Si_3N_4 matrix near the Ta wires, due to the difference in coefficient of thermal expansion between Ta and Si_3N_4 , requiring a higher load to initiate crack extension thus leading to the observed higher K_{IC} values at RT for the Si_3N_4 -Ta composite. However, at 1300°C this residual stress would be very small, and with the Ta wires being very weak at this temperature, a lower K_{IC} value would result.

Also, at elevated temperatures the distance from the crack tips to the first layer of Ta wires does not appear to influence the observed critical stress intensity factor, as it did at RT, with the slightly higher K_{IC} value for sample KC-13 over KC-17 and 18 being due to its lower c/d ratio (0.40 compared to 0.50).

In the fabrication of the notched beam specimens, it became apparent that in order to notch the sample accurately to within a prescribed distance from the first layer of Ta wires, the exact placement of the Ta wires within the sample must be known. In order to determine this, each as-pressed sample was subjected to X-radiography which delineated the position of the Ta wires very precisely. The sample was then ground to size and notched. The estimated distance from the notch tip to the Ta wires, as determined from the radiographs, was usually very close to the actual distance as measured after testing. Figure 24 shows typical radiographs of as-pressed samples to be used for notched beam tests (top) and short beam shear tests (bottom). In the latter case, two samples could be obtained from one hot press by separating two sets of Ta wires in the Si_3N_4 matrix and then cutting the sample in half.

The use of X-radiography in the Si_3N_4 -Ta system allows very accurate measurement of the position of the Ta wire reinforcement and thus subsequent machining of complicated shapes, such as a turbine vane, could be done without exposing any of the Ta wires. This tool was also used to assist in fabrication of Si_3N_4 -Ta double torsion and tensile test samples.

4.2 Double Torsion Tests

The specimen configuration used in double torsion tests is shown in Fig. 25. This specimen gives a constant K being independent of crack length and the long crack lengths attainable are particularly useful for slow crack growth tests.

The double torsion method was devised by Outwater (Ref. 21) who used a traveling microscope to measure the rate of crack growth under a constant applied load. The method was improved and extended by Evans (Refs. 22,23) who showed that at a constant displacement (or constant displacement rate) the crack growth may be obtained directly from the load P or the load relaxation rate dP/dT . This is the basis of the compliance technique, and it is this development that makes the double torsion test so useful. Two approaches are available, the constant displacement method or the constant displacement-rate (constant load) method. The former method was initially chosen for this investigation into the crack growth rates of Si_3N_4 and Si_3N_4 -Ta composites. The derivation of the crack velocity equation for the constant displacement method is detailed by Braiden (Ref. 24) and will not be repeated here. The crack velocity equation thus derived is given as:

$$\frac{da}{dt} = - \frac{P_f}{P^2} a_f \frac{dp}{dt}$$

where da/dt = crack velocity
 P_f = final load
 P = initial load
 a_f = final crack length
 dp/dt = load relaxation rate.

The crack velocity can thus be found if the initial and final loads, the load relaxation with time, and the final crack length can be found.

Prior to conducting crack growth tests on Si_3N_4 and Si_3N_4 -Ta composites, a series of calibration tests were run with glass slides to verify the test equipment and procedures. The results of these tests agreed very well with previous data published by Evans (Ref. 22) and Calvert (Ref. 25). Thus, tests were initiated on double torsion samples of Si_3N_4 (both NC-132 and UTRC Si_3N_4 + 15% Y_2O_3) and Si_3N_4 -Ta composite.

It became obvious early on in the double torsion testing that hot-pressed Si_3N_4 at RT exhibits crack growth by unstable propagation and arrest with little evidence of stable subcritical crack propagation. These observations are confirmed by Tressler, et al (Ref. 19).

After many futile efforts trying to propagate a crack by the constant displacement method, it was decided to use the constant load technique. To compute K_I vs da/dt for this method, one needs to know the initial crack length (a_i), the final crack length (a_f), and the time (t) it takes to propagate the crack this distance for a given load (P). The stress intensity factor can then be calculated from the equation given in Fig. 25:

$$K_I = P W_m \left[\frac{3(1+\nu)}{W t^3 t_n} \right]^{1/2}$$

where P = total applied load

W_m = specimen moment arm (0.731")

ν = Poisson's ratio (0.25)

W = specimen width (1.00")

t = specimen thickness (0.100")

t_n = specimen thickness to notch (0.085")

The results obtained at UTRC for a limited number of tests at RT for Norton NC-132 and UTRC $\text{Si}_3\text{N}_4 + 15\% \text{Y}_2\text{O}_3$ are plotted in Fig. 26, along with data from Calvert (Ref. 25) for NC-132 at 927°C. No K vs V curves for hot-pressed Si_3N_4 at RT were found in the literature. Due to the extreme scatter obtained for crack velocity vs K_I for both the NC-132 and $\text{Si}_3\text{N}_4 + 15\% \text{Y}_2\text{O}_3$ samples, no curves have been drawn through the data points obtained at RT. The only statement that can be made unequivocally is that to initiate crack propagation and to sustain a given crack velocity requires a significantly higher load for the yttria additive Si_3N_4 than for the NC-132 Si_3N_4 with MgO additive, i.e. to maintain a crack velocity of $\sim 1 \times 10^{-6}$ m/sec in yttria additive Si_3N_4 requires a constant load of ~ 60 lbs compared to ~ 40 lbs for the same velocity in NC-132 Si_3N_4 . This correlates well with the observed higher K_{IC} values for yttria additive Si_3N_4 over NC-132 Si_3N_4 determined from notched beam tests at RT, as reported previously.

The Ta reinforced Si_3N_4 double torsion specimen tested at RT consisted of a 2.25 in. long sample with Ta wires (one layer) in the center 0.80 in. A radiograph of this sample is shown in Fig. 27. There were 12, 25 mil Ta wires at an average spacing of 40 mils apart with the first wire being 0.725 in. from the notched end of the sample. All samples contained a 0.055 in. wide by 0.015 in. deep notch down the center and a 0.008 in. wide curved notch extending 0.100 in. into the top surface and 0.300 in. into the bottom (longitudinally notched) surface. The top surface was polished to a mirror finish so that crack length could be measured optically.

No data were obtained for the Ta reinforced $\text{Si}_3\text{N}_4 + 15\% \text{Y}_2\text{O}_3$ specimen at RT since at no time did continuous crack growth occur at RT. However, it did take a significantly higher load to propagate the crack out of the presawn notch for this sample than for the unreinforced $\text{Si}_3\text{N}_4 + 15\% \text{Y}_2\text{O}_3$ sample. A load of 104 lbs was required to initiate crack propagation in this sample compared to ~70 lbs in the unreinforced sample. The crack propagated in one jump to a distance of 0.350 in. where it stopped, approximately 0.375 in. from the first Ta wire. The load was then held at 100 lbs for 81 minutes with no crack growth occurring when the crack suddenly moved to a distance of 0.912 in. which was approximately to the third Ta wire. The sample was then reloaded to 60 lbs and held for 15 minutes with no further crack growth occurring. At this time the load was slowly increased to 64 lbs when the crack suddenly propagated completely through the sample. The Ta wires remained intact with the crack simply moving around them. Due to the discontinuous nature of crack propagation in this sample, it is felt that no meaningful conclusions can be drawn.

Elevated temperature crack growth tests at 1300°C were done on $\text{Si}_3\text{N}_4 + 15\% \text{Y}_2\text{O}_3$ samples, with and without Ta wire reinforcement. The lower fixture that the double torsion plate rested upon was fabricated from hot pressed NC-203 SiC while the upper loading fixture and rams were made of molybdenum. All testing at 1300°C was done in an argon environment. At this temperature, continuous crack growth was observed in both reinforced and unreinforced samples. Crack lengths were measured by removing the sample from the furnace after each run and applying a load at RT so that the reflection of a light source on the polished surface of the sample would identify the tip of the crack.

The data points obtained are plotted in Fig. 28 along with K_I vs da/dt for HS-130 Si_3N_4 at 1300°C as reported by Evans, et al (Ref. 26). Insufficient data were obtained to plot actual K vs V curves for $\text{Si}_3\text{N}_4 + 15\% \text{Y}_2\text{O}_3$, with and without Ta wires, but it appears that the crack growth rates for the two materials fall within the scatter band for HS-130, as determined by Evans, et al, except for one point for the Si_3N_4 -Ta composite. The composite sample contained 20 wires in the center $1 \frac{1}{4}$ in. of the $2 \frac{1}{4}$ in. long specimen, with the three data points plotted in Fig. 28 representing crack growth from the third to the eighth wire, the eighth to the ninth, and the ninth to the eleventh. It was the last measurement from the ninth to eleventh wire, done under a fairly high load of 80 lbs (K_I of $6.75 \text{ MN/m}^{3/2}$) that gave a very low value for the crack growth rate. It is apparent that further tests would be necessary to obtain sufficient data to plot meaningful K_I vs V curves.

From the limited number of tests done on Si_3N_4 -Ta composite samples, it can be concluded that the presence of the Ta wires is not detrimental to the crack growth rates at RT or 1300°C (inert atmosphere). It cannot be said at this time, however, whether or not the Ta wire reinforcement is actually helpful in slowing down or blunting the crack as it moves through the material.

V. CONCLUSIONS

The conclusions that can be reached from the fifth and final year of work on this contract are:

1. The elastic modulus of $\text{Si}_3\text{N}_4 + 15\% \text{Y}_2\text{O}_3$ reinforced with 24 vol %, 25 mil Ta wires as measured in RT 4-pt bending with the first layer of Ta wires within 15 mils of the tensile surface is 36.7×10^6 psi (253 GPa). With the first layer of wires 40 mils from the tensile surface the RT elastic modulus measured 44.5×10^6 psi (307 GPa).
2. The elastic modulus of $\text{Si}_3\text{N}_4 + 15\% \text{Y}_2\text{O}_3$ reinforced with 25 vol %, 25 mil Ta wires as measured by an ultrasonic pulse echo test is 41.5×10^6 psi (287 GPa) at RT, falling to 38.7×10^6 psi (267 GPa) at 1050°C.
3. The thermal expansion coefficient of $\text{Si}_3\text{N}_4 + 15\% \text{Y}_2\text{O}_3$ hot-pressed material was measured as $2.9 \times 10^{-6}/^\circ\text{C}$ from RT to 925°C and $3.4 \times 10^{-6}/^\circ\text{C}$ from RT to 1300°C. The corresponding values for this matrix reinforced with 25 vol % Ta wires are $3.2 \times 10^{-6}/^\circ\text{C}$ and $3.8 \times 10^{-6}/^\circ\text{C}$.
4. The thermal conductivity of a $\text{Si}_3\text{N}_4 + 20$ vol %, 25 mil Ta composite in the direction parallel to the Ta wires was measured as $47 \text{Wm}^{-1} \text{K}^{-1}$ at 50°C, falling gradually to $22 \text{Wm}^{-1} \text{K}^{-1}$ at 1000°C. These values are 42% and 16% higher, respectively, than the thermal conductivity measured for monolithic hot-pressed Si_3N_4 .
5. The Si_3N_4 -Ta composite system is difficult to fail in short beam shear at both RT and 1300°C. All samples tested failed essentially in tension (bending) with a few RT samples exhibiting some secondary shear component.
6. The ultimate tensile strength of $\text{Si}_3\text{N}_4 + 15\% \text{Y}_2\text{O}_3$ was measured as ~80 ksi (550 MPa) at RT and 61 ksi (420 MPa) at 1300°C. Tantalum reinforced Si_3N_4 exhibited a very low RT UTS value of 24 ksi (165 MPa).
7. The critical stress intensity factor (K_{IC}) measured from the notched beam test at RT with a constant crack depth to sample thickness ratio (c/d) of 0.50 for monolithic $\text{Si}_3\text{N}_4 + 15\% \text{Y}_2\text{O}_3$ increases from $4.94 \text{MN/m}^{3/2}$ at 97% density to $5.68 \text{MN/m}^{3/2}$ at 99+% density, with further increases to $6.75 \text{MN/m}^{3/2}$ at longer hot-pressing times (1 hr).
8. Norton NC-132 Si_3N_4 tested at a c/d of 0.50 gives a RT K_{IC} value of $4.71 \text{MN/m}^{3/2}$.

9. The K_{IC} value at RT of $Si_3N_4 + 15\% Y_2O_3$ reinforced with Ta wires was measured at $8.57 MN/m^{3/2}$, a 25% increase over comparable monolithic Si_3N_4 material. The notch tip to Ta wire distance in this sample was only 3 mils.

10. The K_{IC} of monolithic $Si_3N_4 + 15\% Y_2O_3$ measured by the notched beam test at $1300^\circ C$ varies from $5.30 MN/m^{3/2}$ to $8.00 MN/m^{3/2}$, with more fully dense specimens (99%+) yielding higher values.

11. The K_{IC} of Ta reinforced $Si_3N_4 + 15\% Y_2O_3$ at $1300^\circ C$ averages $5.06 MN/m^{3/2}$, significantly lower than that measured at RT. This could be due to a state of compressive prestress existing in the Si_3N_4 matrix at RT which is relieved at elevated temperature.

12. The use of X-radiography to determine the location of the Ta wires in Si_3N_4 -Ta composites allows accurate grinding and cutting of complex shapes without exposing the Ta wires.

13. The crack growth rates for $Si_3N_4 + 15\% Y_2O_3$, as measured by a limited number of double torsion tests, appear to be less for a given stress intensity than Norton NC-132 Si_3N_4 at RT and about the same as Norton HS-130 at $1300^\circ C$. $Si_3N_4 + 15\% Y_2O_3 + Ta$ wire composite samples appear to have crack growth rates similar to, if not lower than, unreinforced samples of the same matrix at RT and $1300^\circ C$.

VI. ACKNOWLEDGEMENTS

The author would like to thank Dr. Frank C. Douglas for his technical assistance in performing the thermal expansion, elastic modulus, and double torsion crack growth studies and also Dr. Charles O. Hulse for his assistance and advice in performing the tensile and crack growth tests. This work has been supported by the Naval Air Systems Command under the direction of Mr. Irving Machlin.

REFERENCES

1. Norton Co. Brochure, "Ceramics for Engine Components", hot-pressed NC-132 Si_3N_4 property data.
2. G. E. Gazza, "Effect of Yttria Additions on Hot Pressed Si_3N_4 ", presented at Am. Cer. Soc. Meeting, Chicago, IL, April 30, 1974.
3. A. Tsuge, K. Nishida, and M. Komatsu, "Effect of Crystallizing the Grain-Boundary Phase on the High Temperature Strength of Hot-Pressed Si_3N_4 Containing Y_2O_3 ", J. Am. Cer. Soc., Vol. 58, No. 7-8, July-August 1975.
4. J. E. Ashton, J. C. Halpin, P. H. Petit, "Primer on Composite Materials: Analysis", p. 85, Technomic Publishing Co., Stratford, CT, 1969.
5. "Thermophysical Properties of High Temperature Solid Materials", Vol. 1: Elements, p. 936, edited by Y. S. Touloukian, Purdue Univ., MacMillan Publishing Co., NY, 1967.
6. R. P. Tye, J. Less Common Metals, 3, pp 202-215.
7. D. W. Richarson, "ARPA/Navy Ceramic Engine Materials and Process Development Summary", presented at the Fifth Army Materials Technology Conference on "Ceramics for High Performance Applications-II", Newport, RI, March 21-25, 1977.
8. Pratt & Whitney Aircraft Internal Report EII-74-243-0003, reported by C. G. Nessler, March 1974.
9. R. J. Bratton, D. G. Miller, "Summary of ARPA Stationary Turbine Project", presented at the Fifth Army Materials Technology Conference on "Ceramics for High Performance Applications-II", Newport, RI, March 21-25, 1977.
10. F. F. Lange, "High Temperature Strength Behavior of Hot-Pressed Si_3N_4 : Evidence for Subcritical Crack Growth", J. Am. Cer. Soc. (57), 2, p 84, Feb. 1974.
11. S. M. Wiederhorn, "Subcritical Crack Growth in Ceramics", Fracture Mechanics of Ceramics, Vol. 2, p 613, edited by Bradt, Hasselman, and Lange, Plenum Press, NY, 1974.
12. H. R. Baumgartner and P. E. Cowley, "Silicon Nitride in Rolling Contact Bearings", Final Rept. on NASC Contract N00019-74-C-0157, July 15, 1975.
13. W. F. Brown, Jr. and J. E. Srawley, "Plane Strain Crack Toughness Testing of High-Strength Metallic Materials", Am. Soc. Test. Mat., Special Tech. Publ. #410, 1966, pp 13-15.

14. D. A. Summers, J. Corwine, and Li-King Chen, "Comparison of Methods Available for Determination of Surface Energy", pp 241-61 in Proc. 12th Symp. on Rock Mech., 1970.
15. S. D. Hartline, R. C. Bradt, H. R. Baumgartner, and N. B. Rosebrooks, "Notched-Beam Test for Fracture Energy Measurement", J. Am. Cer. Soc., Vol. 56, NO. 10, Oct. 1973.
16. N. Claussen and C. P. Lahmann, "Fracture Behavior of Some Hot-Pressed Si_3N_4 Ceramics at High Temperatures", Powder Met. Intl., Vol. 7, No. 3, 1975.
17. D. R. Messier and F. L. Riley, "Interconversion of the α and β Phases of Si_3N_4 ", presented at the NATO-ASI "Nitrogen Ceramics", Canterbury, England, Aug. 1976.
18. J. L. Iskoe and F. F. Lange, "Development of Microstructure, Strength and Fracture Toughness of Hot-Pressed Si_3N_4 ", Tech. Rept. #7, ONR Contract N00014-74-C-0284, April 1, 1976.
19. R. E. Tressler, T. Yonushonis, and M. Meiser, "Crack Propagation in, and Molten Salt Corrosion of, Si_3N_4 ", presented at the NATO-ASI "Nitrogen Ceramics", Canterbury, England, Aug. 1976.
20. J. A. Coppola, R. C. Bradt, D. W. Richerson, and R. A. Alliegro, "Fracture Energy of Silicon Nitrides", Am. Cer. Soc. Bull., Vol. 51, No. 11 (1972) p. 847.
21. J. O. Outwater and D. J. Jerry, "On the Fracture Energy of Glass", Interim Report Contract NONR-3219 (ONX), Univ. of Vermont, 1966.
22. A. G. Evans, "A Simple Method for Evaluating the Time-Dependent Failure Characteristics of Brittle Materials", J. Mat. Sci. 7, (1972) p 1137.
23. D. P. Williams and A. G. Evans, "A Simple Method for Studying Slow Crack Growth", J. of Testing and Evaluation, 1 (4), 1973, p 264.
24. P. M. Braiden, "Fracture Mechanics of High Temperature Ceramics", AGARD Report No. 651 on Mechanical Properties of Ceramics for High Temperature Applications, Dec. 1976, p 27.
25. G. S. Calvert, "Design, Fabrication and Spin Testing of Ceramic Blade-Metal Disk Attachment", Quarterly Report No. 3 on Contract NAS3-19715, April 15, 1976.
26. A. G. Evans and S. M. Wiederhorn, "Crack Propagation and Failure Prediction in Si_3N_4 at Elevated Temperatures", J. Mat. Sci. 9, 1974, pp 270-278.

Table I

Thermal Expansion Coefficients for $\text{Si}_3\text{N}_4 + 15\% \text{Y}_2\text{O}_3$
and $\text{Si}_3\text{N}_4 + 15\% \text{Y}_2\text{O}_3 - 25 \text{ vol } \% \text{Ta}$

<u>Material</u>	<u>Average Coefficient of Thermal Expansion</u>	
	<u>20°-925°C</u>	<u>20°-1300°C</u>
$\text{Si}_3\text{N}_4 + 15\% \text{Y}_2\text{O}_3$	$2.9 \times 10^{-6}/^\circ\text{C}$	$3.4 \times 10^{-6}/^\circ\text{C}$
$\text{Si}_3\text{N}_4 + 15\% \text{Y}_2\text{O}_3 - 25 \text{ vol } \% \text{Ta}$	$3.2 \times 10^{-6}/^\circ\text{C}$	$3.8 \times 10^{-6}/^\circ\text{C}$

Table II

Thermal Conductivity of Si_3N_4 and 20 vol % Ta
Reinforced Si_3N_4 ($\text{Wm}^{-1} \text{K}^{-1}$)

<u>Temperature °C</u>	<u>NC-132</u>	<u>Si_3N_4-Ta longitudinal, measured</u>	<u>Si_3N_4-Ta longitudinal, calculated</u>	<u>Si_3N_4-Ta transverse, calculated</u>
50	33	47	38.2	49.5
200	30	39	35.8	45.0
400	27	32	33.4	40.5
600	23	27	30.2	34.5
800	21	24	28.6	31.5
1000	19	22	27.0	28.5

Table III

Short Beam Shear Tests of Si_3N_4 + 25 vol %, 25 mil Ta

<u>Sample No.</u>	<u>Temp °C</u>	<u>Span/Depth</u>	<u>(ksi)</u>	<u>(MPa)</u>	<u>Failure Mode</u>
SNT-1a	RT	5/1	>9.5	>65.3	Bending, some secondary shear component
-1b	RT	5/1	>10.6	>73.1	Bending, some secondary shear component
-2a	RT	5/1	>13.2	>90.7	Bending
-2b	RT	5/1	>12.7	>87.8	Bending
-3a	RT	4/1	>11.8	>81.6	Bending
-3b	RT	3/1	>15.1	>104	Bending
-4b	RT	Compressive Shear	>15.5	>107	Ram failed
-5a	1300	5/1	>4.45	>30.7	Bending
-5b	1300	5/1	>3.76	>25.9	Bending, some secondary shear component
-6a	1300	4/1	>4.55	>31.3	Bending

Table IV

Uniaxial Tensile Strength of $\text{Si}_3\text{N}_4 + 15\% \text{Y}_2\text{O}_3$ and
 $\text{Si}_3\text{N}_4 + 15\% \text{Y}_2\text{O}_3$ -Ta Wire Composites

<u>Sample No.</u>	<u>Material</u>	<u>Test Temp</u> °C	<u>UTS at Minimum Cross-Section</u>		<u>UTS at Point of Fracture</u>		<u>Comments</u>
			<u>ksi</u>	<u>MPa</u>	<u>ksi</u>	<u>MPa</u>	
UTS-1	$\text{Si}_3\text{N}_4 + 15\% \text{Y}_2\text{O}_3$	RT	86.3	595	75.6	521	Failed at internal flaw
UTS-2	"	RT	88.5	610	83.6	577	"
UTS-3	"	1300	61.0	420	61.0	420	"
UTS-4	$\text{Si}_3\text{N}_4 + 15\% \text{Y}_2\text{O}_3 + \text{Ta}$	RT	24.0	166	24.0	166	Failed at Ta- Si_3N_4 interface
UTS-5	"	1300		No Test			

Table V

RT Critical Stress Intensity Factor (K_{IC}) Determination
of Si_3N_4 and Si_3N_4 -Ta Samples by the Notched Beam Test

<u>Sample No.</u>	<u>Material</u>	<u>c/d Ratio</u>	<u>K_{IC}(MN/m^{3/2})</u>	<u>Comments</u>
KC-1	$Si_3N_4 + 15\% Y_2O_3 + Ta$	0.25	13.95	Notch 25 mils from Ta wires
KC-2	$Si_3N_4 + 15\% Y_2O_3 + Ta$	0.31	3.85	Notch 10 mils into Ta wires
KC-3	$Si_3N_4 + 15\% Y_2O_3$	0.25	6.55	Areas of incomplete densification in sample
KC-4	$Si_3N_4 + 15\% Y_2O_3$	0.60	5.03	Areas of incomplete densification in sample
KC-6	$Si_3N_4 + 15\% Y_2O_3$	0.50	4.94	Hot-pressed 1725°C, 30 min, $\rho = 97\%$ theoretical
KC-7	$Si_3N_4 + 15\% Y_2O_3$	0.50	5.42	Hot-pressed 1750°C, 30 min, $\rho = 98\%$ theoretical
KC-8	$Si_3N_4 + 15\% Y_2O_3$	0.50	5.68	Hot-pressed 1775°C, 30 min, $\rho = 99+\%$ theoretical
KC-9	$Si_3N_4 + 15\% Y_2O_3$	0.50	6.75	Hot-pressed 1775°C, 1 hr, $\rho = 99+\%$
NC-132	Norton Si_3N_4	0.50	4.71	Commercial material
KC-10	$Si_3N_4 + 15\% Y_2O_3 + Ta$	0.50	7.88	Hot-pressed 1775°C, 30 min, notch 10 mils from Ta wires
KC-11	$Si_3N_4 + 15\% Y_2O_3 + Ta$	0.50	8.57	Hot-pressed 1775°C, 1 hr, notch 3 mils from Ta wires

Table VI

1300°C Critical Stress Intensity Factor (K_{IC}) Determination of Si_3N_4
and Si_3N_4 -Ta Samples by the Notched Beam Test

<u>Sample No.</u>	<u>Material</u>	<u>c/d ratio</u>	<u>K_{IC} MN/m^{3/2}</u>	<u>Comments</u>
KC-12	Si_3N_4 + 15% Y_2O_3	0.40	-	Sample broke on heating
KC-13	Si_3N_4 + 15% Y_2O_3 + Ta	0.40	5.36	Hot-pressed 1775°C, 30 min, notch 5 mils from Ta wires
KC-14	Si_3N_4 + 15% Y_2O_3	0.50	-	Sample support failed
KC-15	Si_3N_4 + 15% Y_2O_3	0.50	8.00	Hot-pressed 1775°C, 1 hr, $\rho = 99+\%$
KC-16	Si_3N_4 + 15% Y_2O_3	0.50	5.30	Hot-pressed 1775°C, 1 hr, $\rho = 98.5\%$
KC-17	Si_3N_4 + 15% Y_2O_3 + Ta	0.50	4.70	Hot-pressed 1775°C, 1 hr, notch 15 mils from Ta wires
KC-18	Si_3N_4 + 15% Y_2O_3 + Ta	0.50	5.06	Hot-pressed 1775°C, 1 hr, notch 20 mils from Ta wires

FIG. 1 – RT ELASTIC MODULUS TEST OF NC-132 Si_3N_4
USING ULTRASONIC PULSE ECHOS

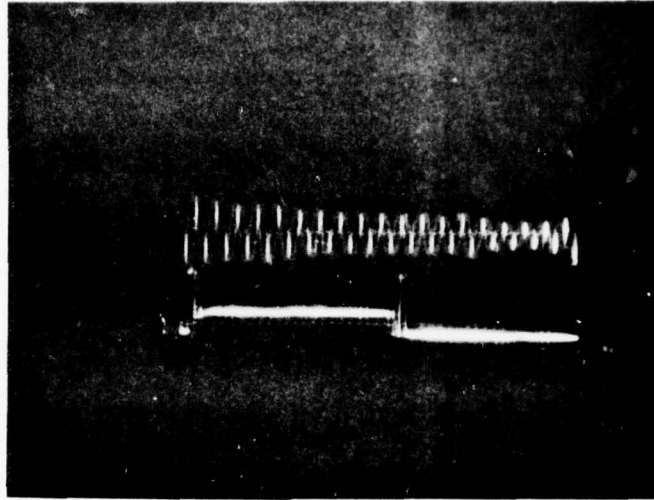


FIG. 2 – RT ELASTIC MODULUS TEST OF Si_3N_4 + Ta WIRE COMPOSITE
USING ULTRASONIC PULSE ECHOS

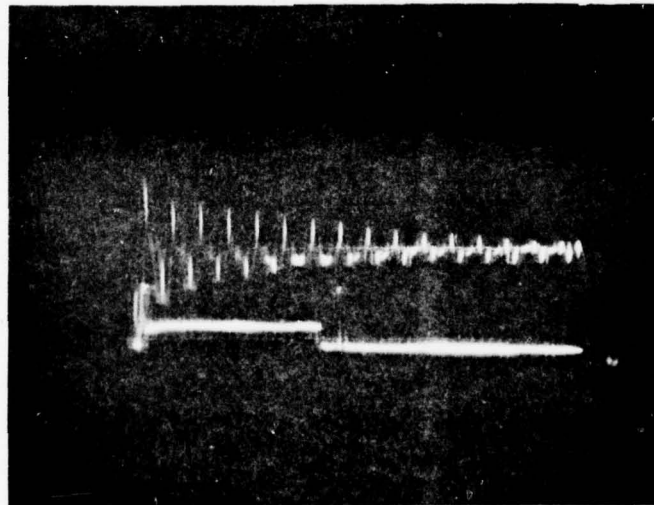


FIG. 3 - ELASTIC MODULUS VS TEMPERATURE FOR NC-132 Si_3N_4 AND Si_3N_4 + 25 VOL% Ta
(ULTRASONIC MEASUREMENT)

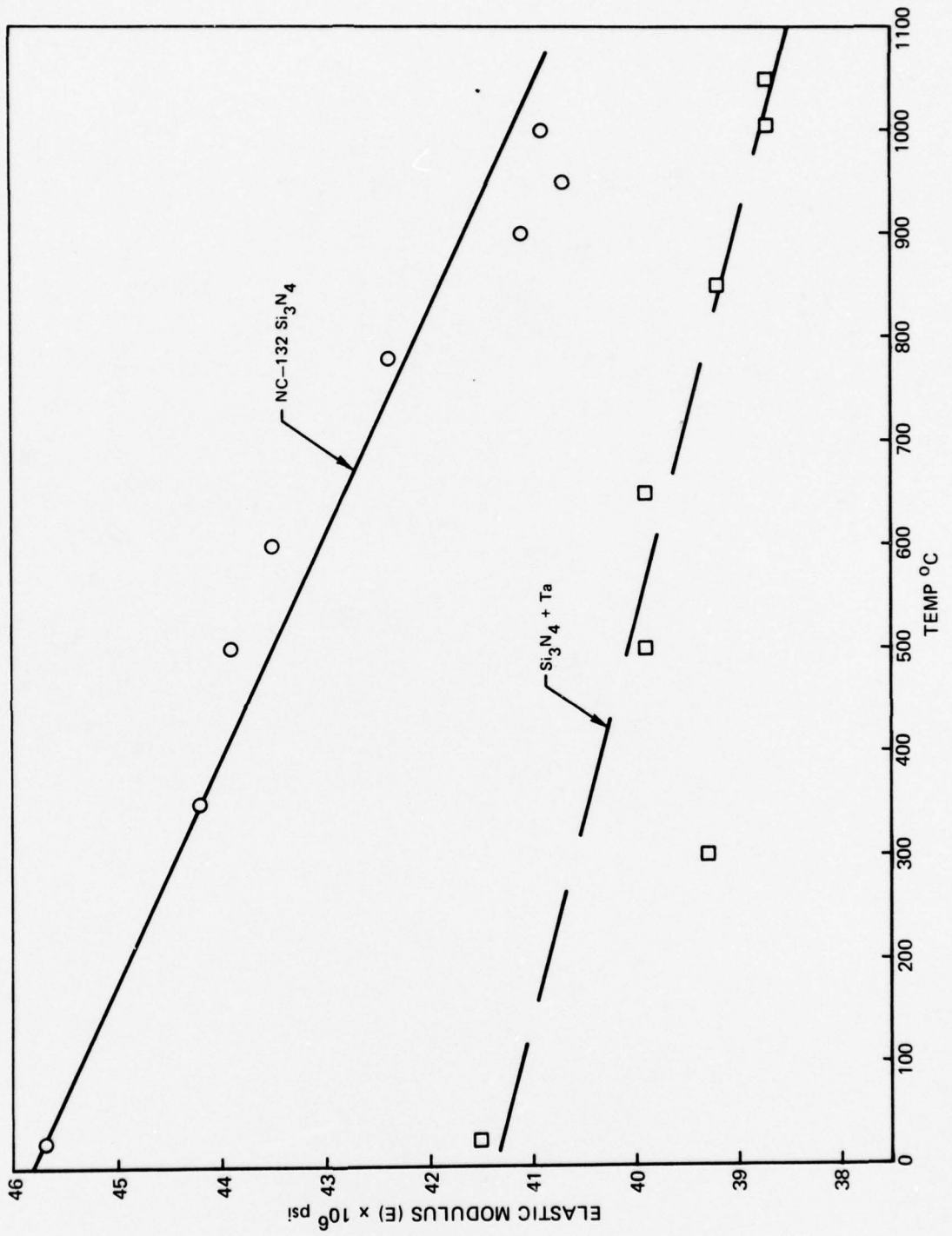


FIG. 4 - THERMAL EXPANSION CURVES FOR $\text{Si}_3\text{N}_4 + 15\% \text{Y}_2\text{O}_3$ AND $\text{Si}_3\text{N}_4 + 15\% \text{Y}_2\text{O}_3 - 25 \text{ VOL } \% \text{Ta TO } 925^\circ\text{C}$

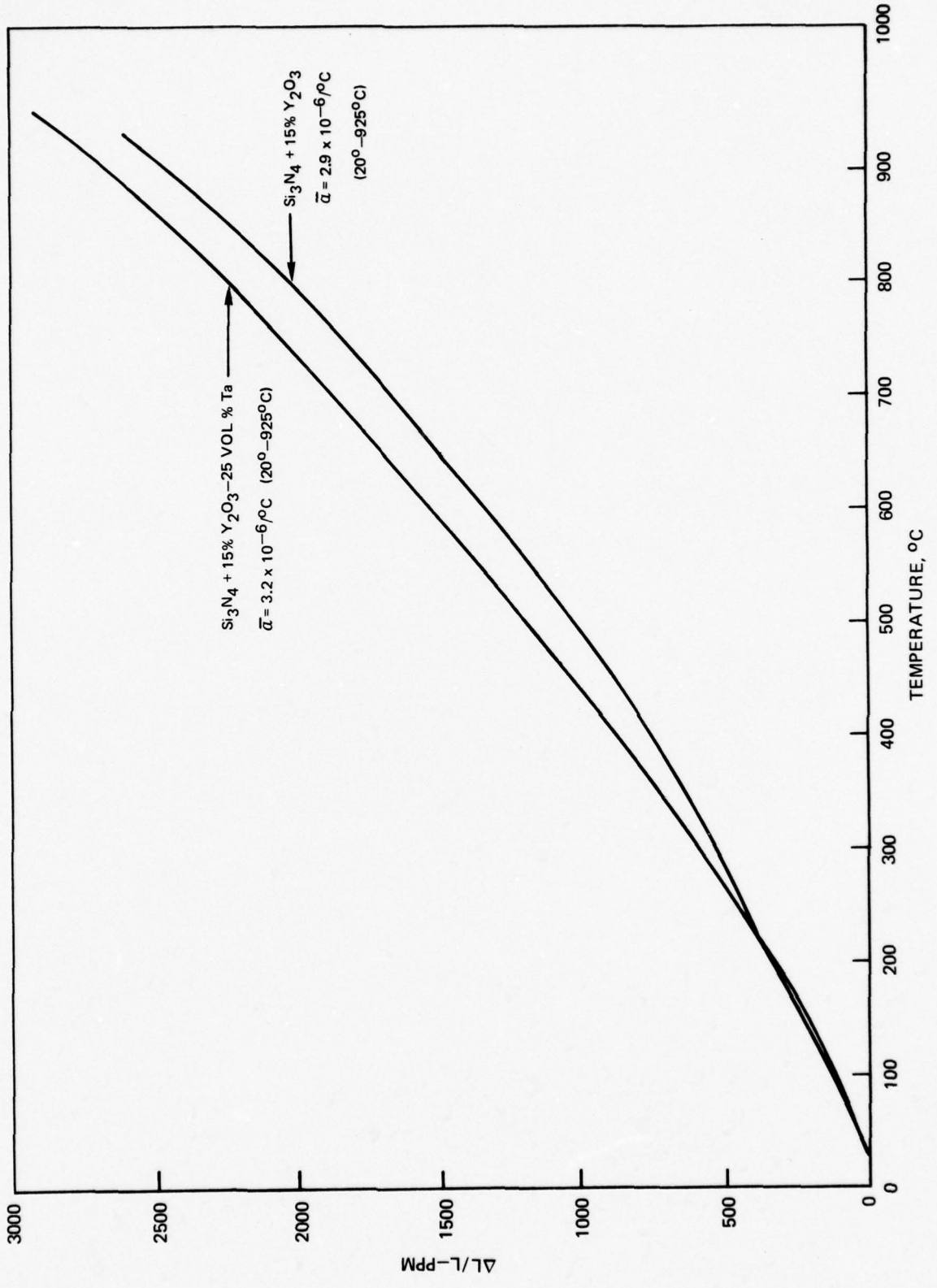


FIG. 5 - THERMAL EXPANSION CURVES FOR $\text{Si}_3\text{N}_4 + 15\% \text{Y}_2\text{O}_3$ AND $\text{Si}_3\text{N}_4 + 15\% \text{Y}_2\text{O}_3 - 25 \text{ VOL } \% \text{Ta}$ TO 1300°C

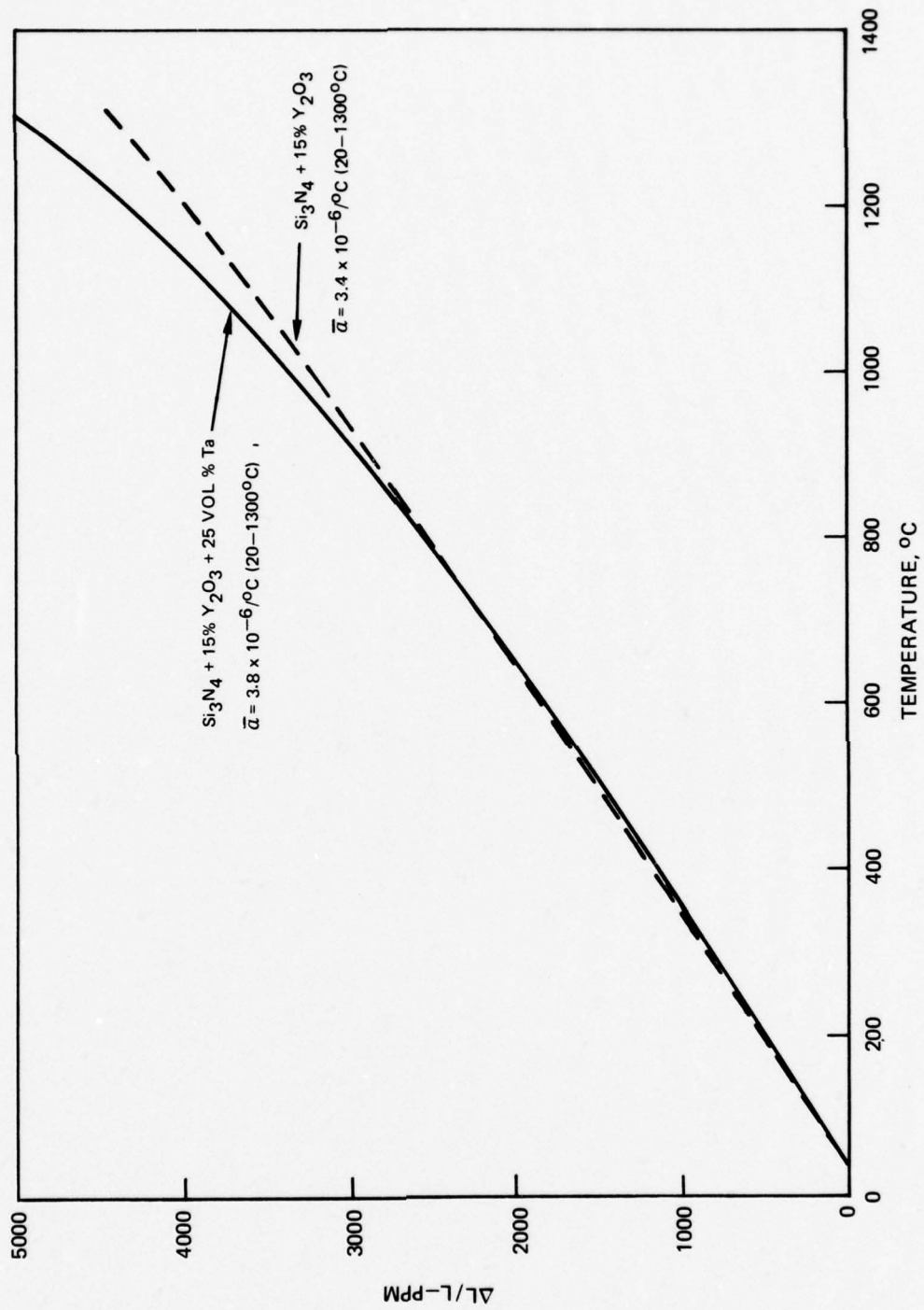


FIG. 6 - THERMAL CONDUCTIVITY VS TEMPERATURE FOR Ta REINFORCED Si_3N_4 AND NORTON NC-132 Si_3N_4

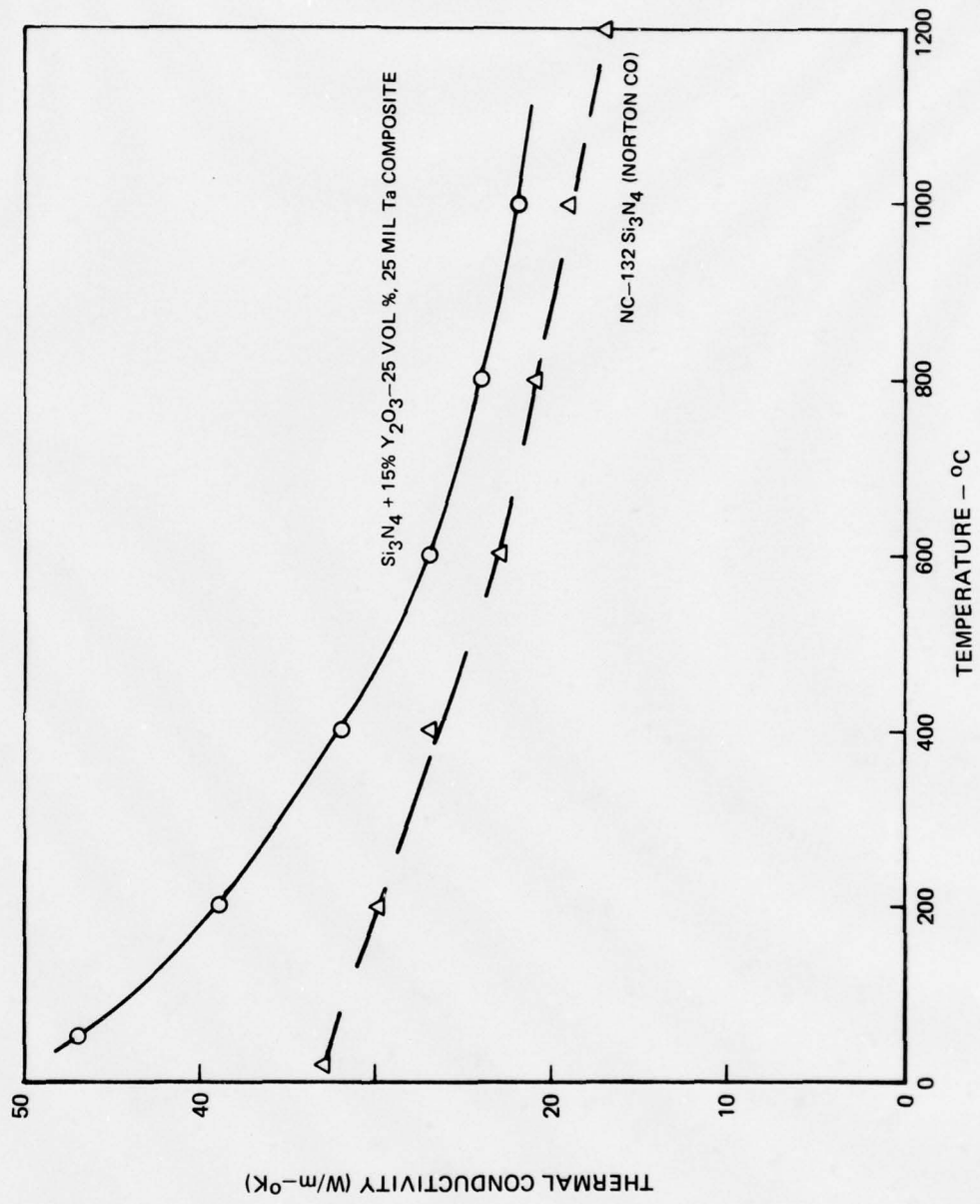


FIG. 7 - RT SHORT BEAM SHEAR SAMPLE OF Si_3N_4 +25 VOL % Ta



FIG. 8 - END OF Si_3N_4 -Ta SHORT BEAM SHEAR SAMPLE SHOWING LONGITUDINAL CRACKS

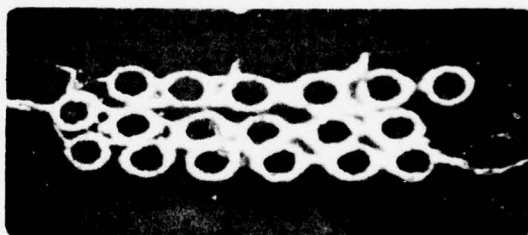


FIG. 9 - UNIAXIAL TENSILE TEST SAMPLE OF $\text{Si}_3\text{N}_4 + 15\% \text{Y}_2\text{O}_3$

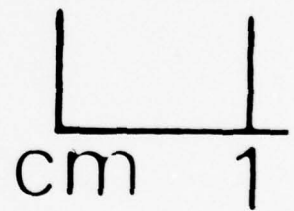


FIG. 10 - FRACTURE SURFACE OF $\text{Si}_3\text{N}_4 + 15\% \text{Y}_2\text{O}_3$ RT TENSILE SAMPLE UTS-2 (20X)

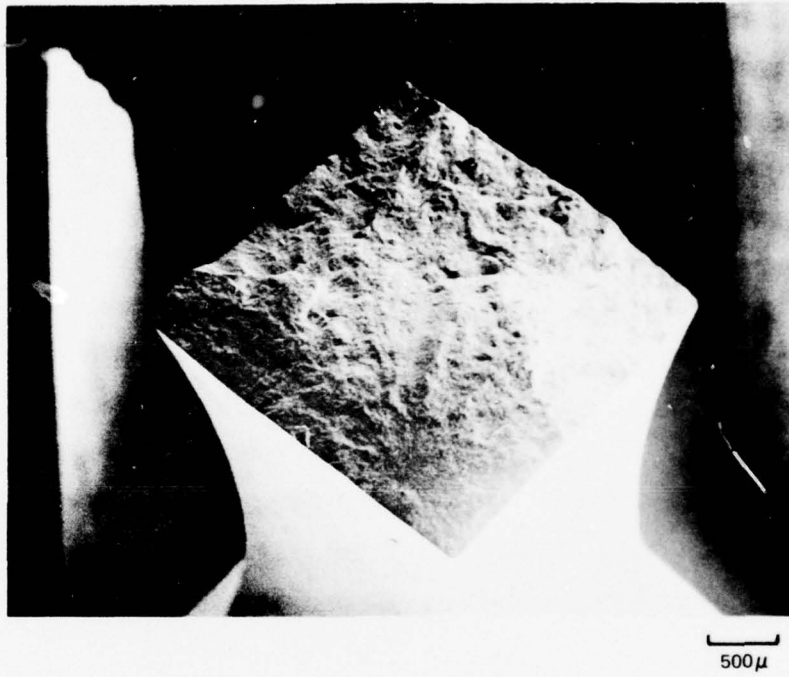


FIG. 11 - FRACTURE SURFACE OF $\text{Si}_3\text{N}_4 + 15\% \text{Y}_2\text{O}_3$ RT TENSILE SAMPLE UTS-2 (100X)

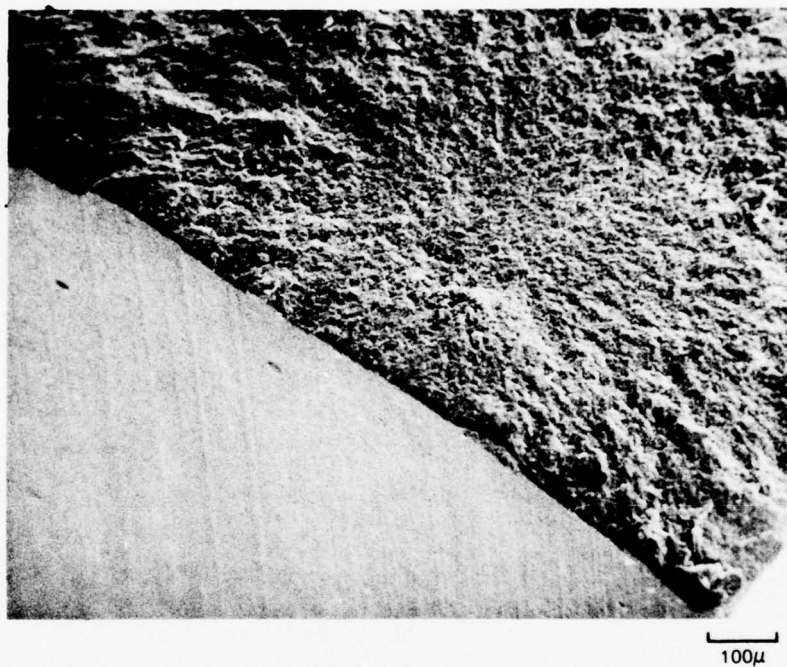


FIG. 12 - FRACTURE ORIGIN OF $\text{Si}_3\text{N}_4 + 15\% \text{Y}_2\text{O}_3$ RT TENSILE SAMPLE UTS-2 (1000X)



10μ

FIG. 13 - SEM OF Si_3N_4 -Ta RT TENSILE FRACTURE SURFACE (50X).

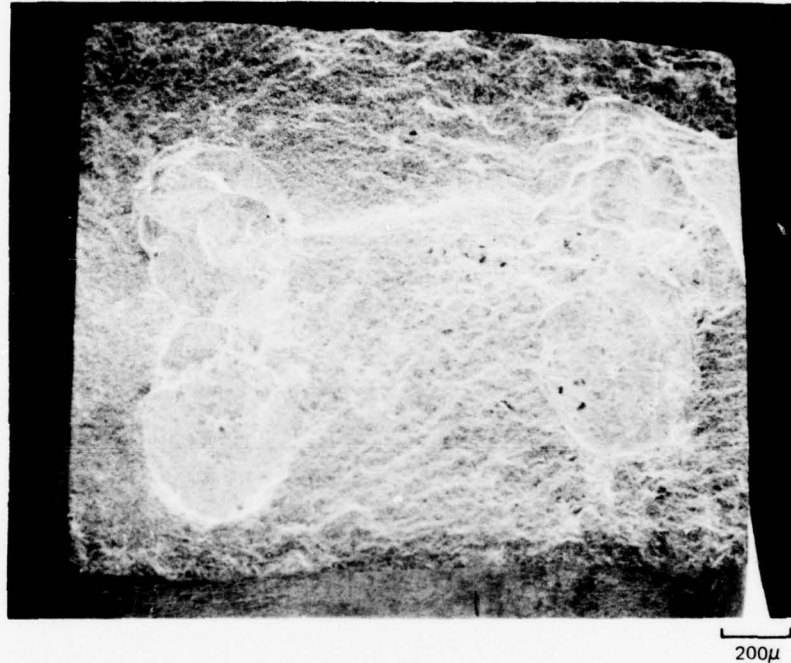


FIG. 14 - SEM OF Si_3N_4 -Ta RT TENSILE FRACTURE SURFACE (100X).

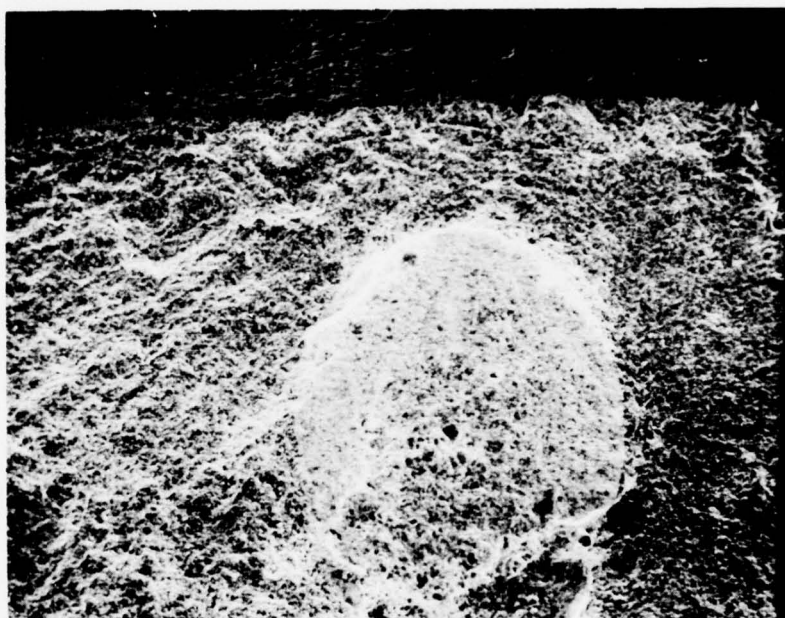
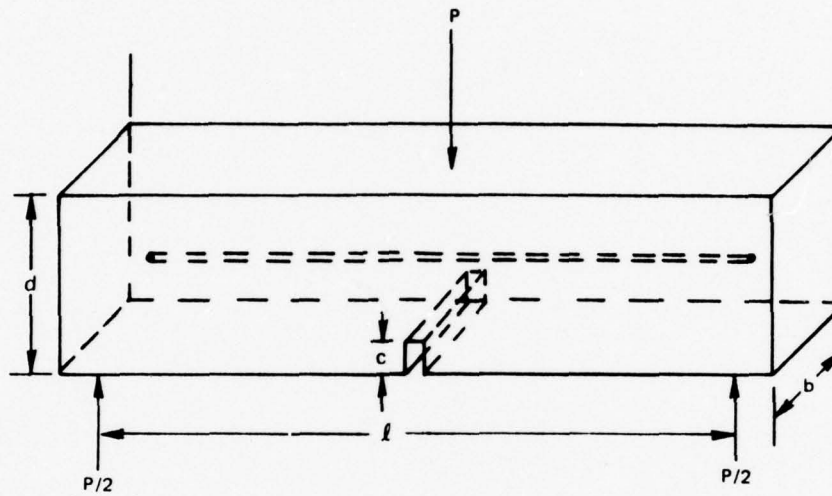


FIG. 15 – BEND SPECIMEN FOR DETERMINING K_{IC} VALUES OF Si_3N_4-Ta COMPOSITES



$$K_{IC} = \frac{3Pl\sqrt{c}}{2bd^2} Y$$

WHERE Y = FUNCTION OF $\frac{c}{d}$

NOTE: ONLY ONE Ta WIRE SHOWN FOR CLARITY

FIG. 16 - FRACTURE SURFACE OF NOTCHED BEAM SAMPLE OF $\text{Si}_3\text{N}_4\text{-Ta}$
(NOTCH 25 MILS FROM Ta WIRES, $K_{IC}=13.95 \text{ MN/m}^{3/2}$)

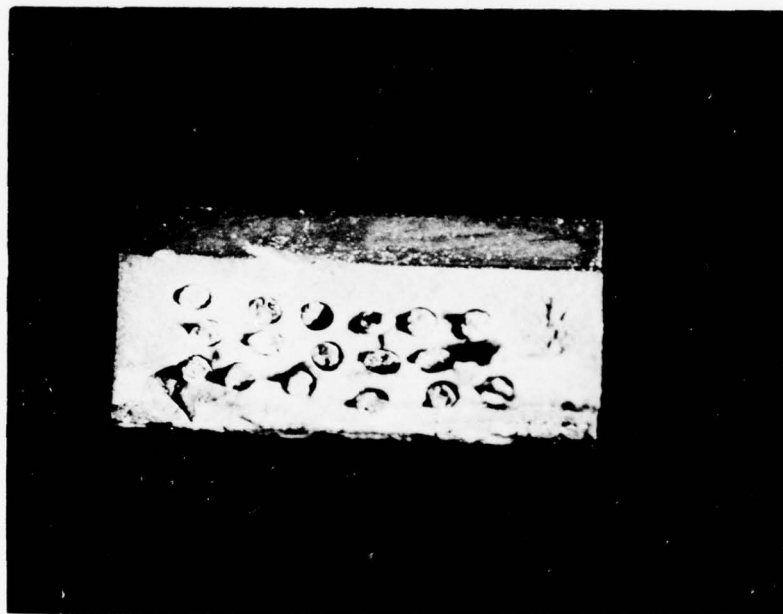


FIG. 17 - FRACTURE SURFACE OF NOTCHED BEAM SAMPLE OF $\text{Si}_3\text{N}_4\text{-Ta}$
(NOTCH 10 MILS INTO Ta WIRES, $K_{IC}=3.85 \text{ MN/m}^{3/2}$)



FIG. 18 - RT NOTCHED BEAM TESTS ON Si_3N_4 (KC-9) AND $\text{Si}_3\text{N}_4+\text{Ta}$ WIRES (KC-11)

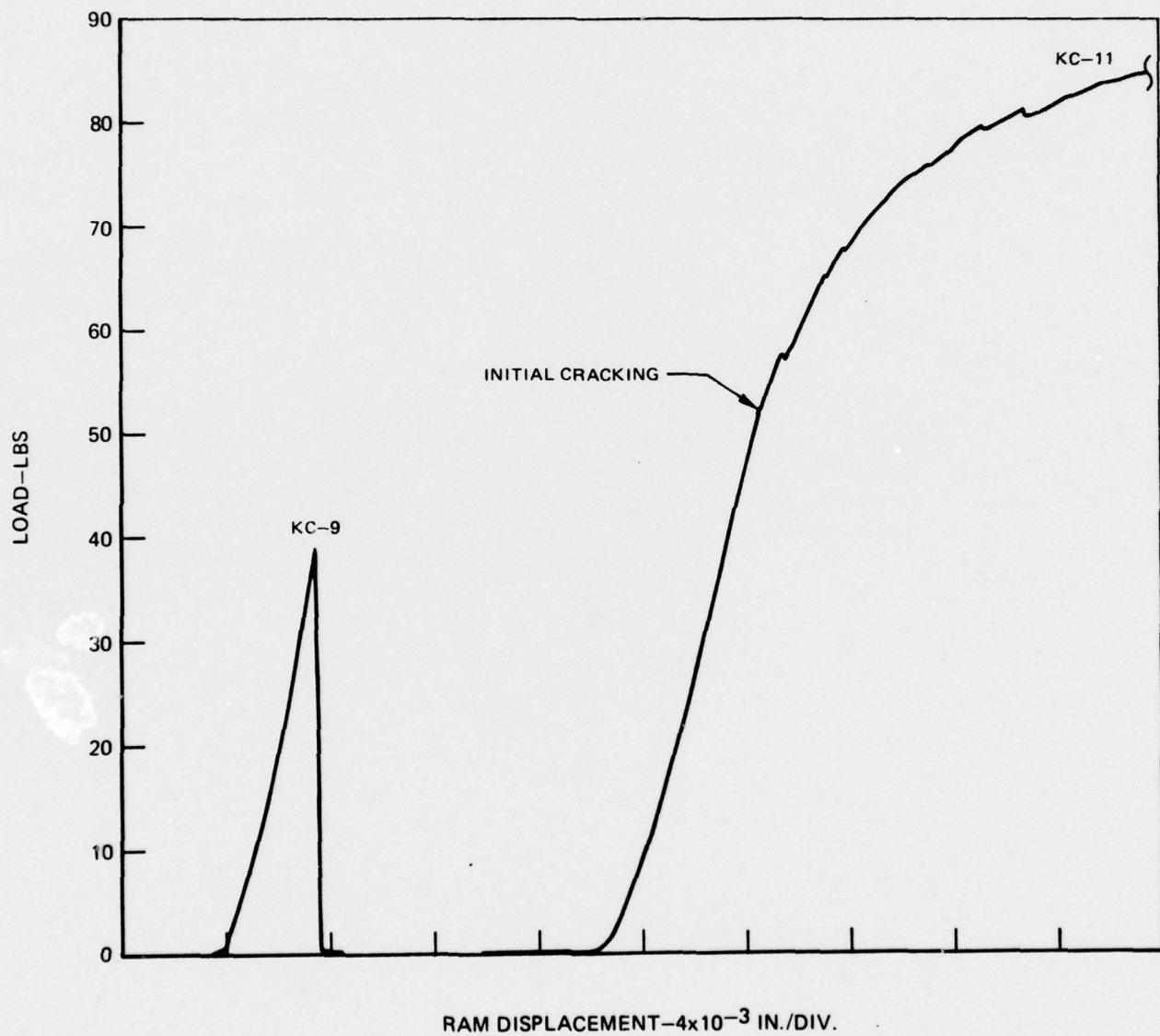


FIG. 19 - NOTCHED BEAM TEST SPECIMENS OF Si_3N_4 -Ta (kC-10, TOP, KC-11, BOTTOM)

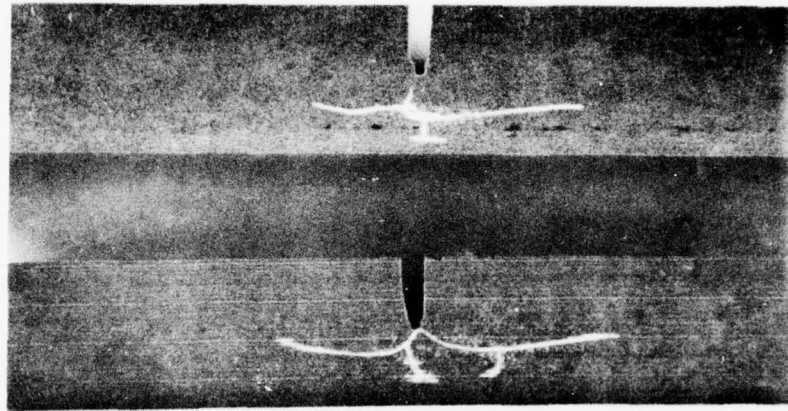


FIG. 20 - FRACTURE SURFACE OF NOTCHED BEAM SAMPLE OF $\text{Si}_3\text{N}_4\text{-Ta}$, KC -10
(NOTCH 10 MILS FROM Ta WIRES, $K_{IC} = 7.88 \text{ MN/m}^{3/2}$)

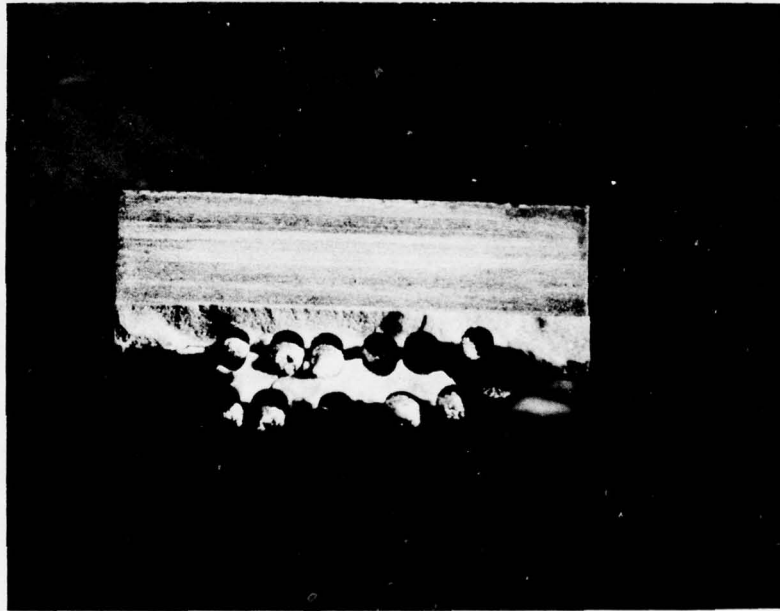


FIG. 21 - FRACTURE SURFACE OF NOTCHED BEAM SAMPLE OF Si_3N_4 - Ta, KC-11
(NOTCHED 3 MILS FROM Ta WIRES, $K_{IC} = 8.57 \text{ MN/m}^{3/2}$)

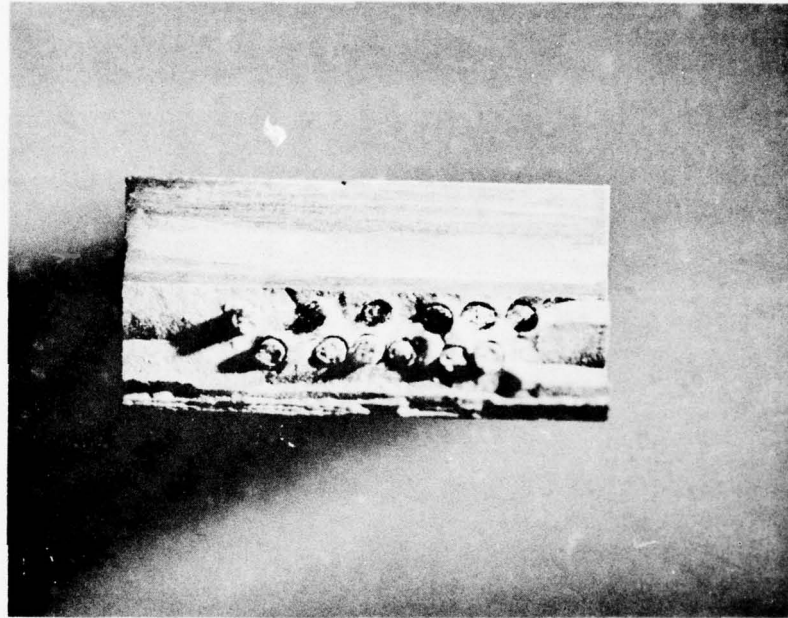


FIG. 22-1300°C NOTCHED BEAM TESTS ON Si₃N₄ (KC-15) AND Si₃N₄ + Ta WIRES (KC-13)

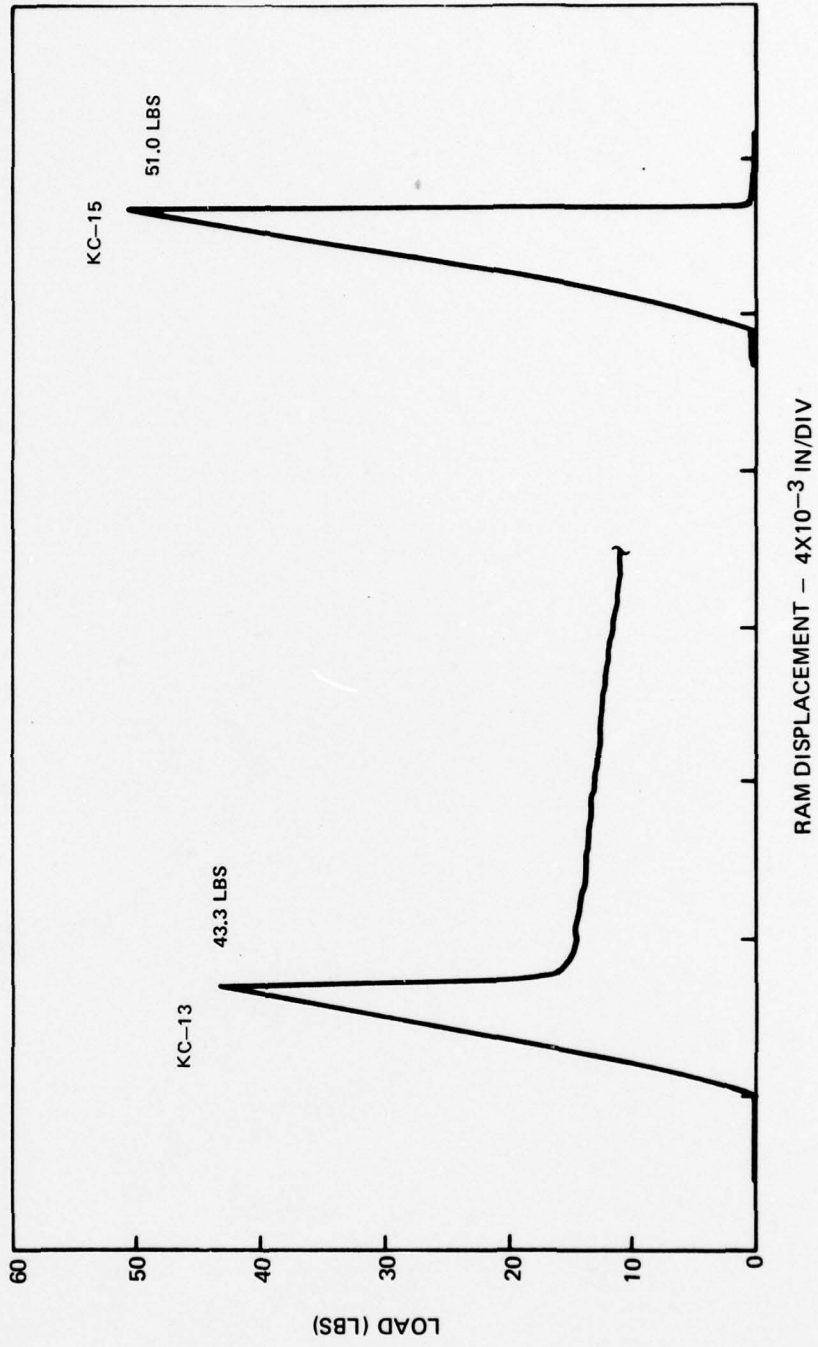


FIG. 23 - FRACTURE SURFACE OF NOTCHED BEAM SAMPLE OF $\text{Si}_3\text{N}_4\text{-Ta}$, KC-13,
(TESTED AT 1300°C , NOTCH 5 MILS FROM Ta WIRES, $K_{IC} = 5.36 \text{ MN/M}^{3/2}$)

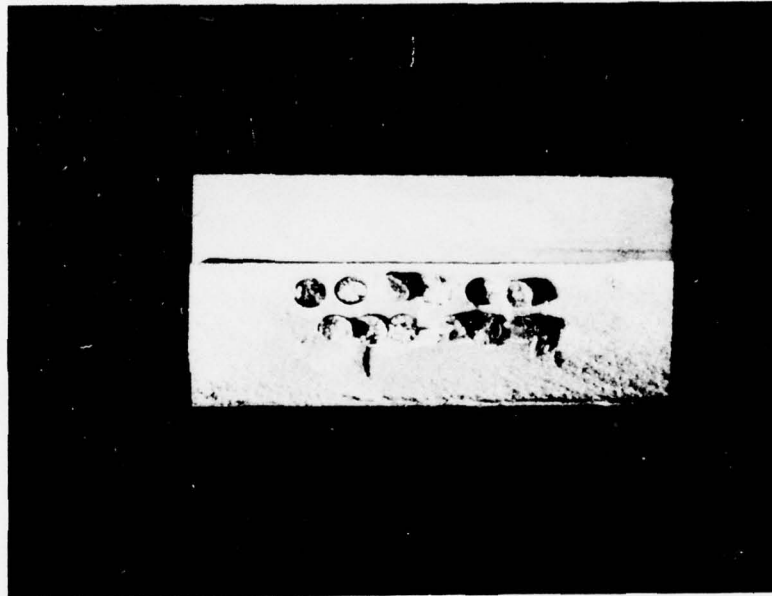
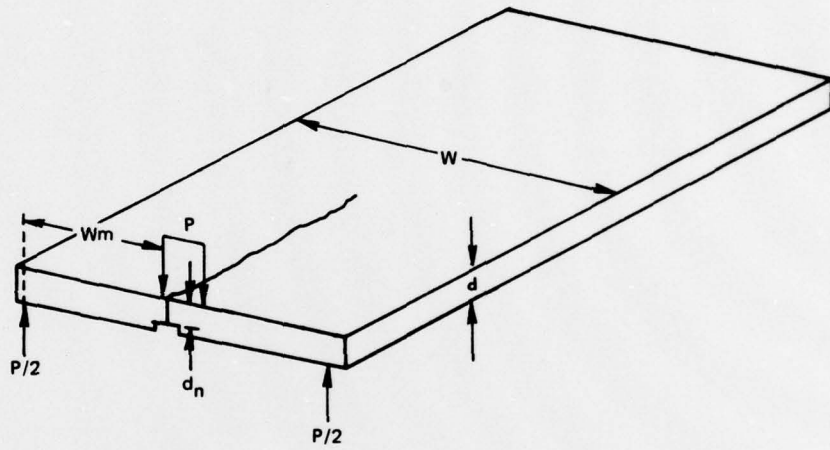


FIG. 24 - X - RADIOGRAPHS OF AS-PRESSED Si_3N_4 -Ta SAMPLES FOR NOTCHED BEAM TESTS (TOP) AND SHORT BEAM SHEAR TESTS (BOTTOM)

2x ORIGINAL SIZE



FIG. 25 - DOUBLE TORSION SPECIMEN FOR DETERMINING CRACK GROWTH RATE AND K_{IC}



$$K_I = PW_m \left[\frac{3(1+\nu)}{Wd^3d_n} \right]^{1/2}$$

FIG. 26—CRACK VELOCITY VS STRESS INTENSITY FOR HOT-PRESSED Si_3N_4

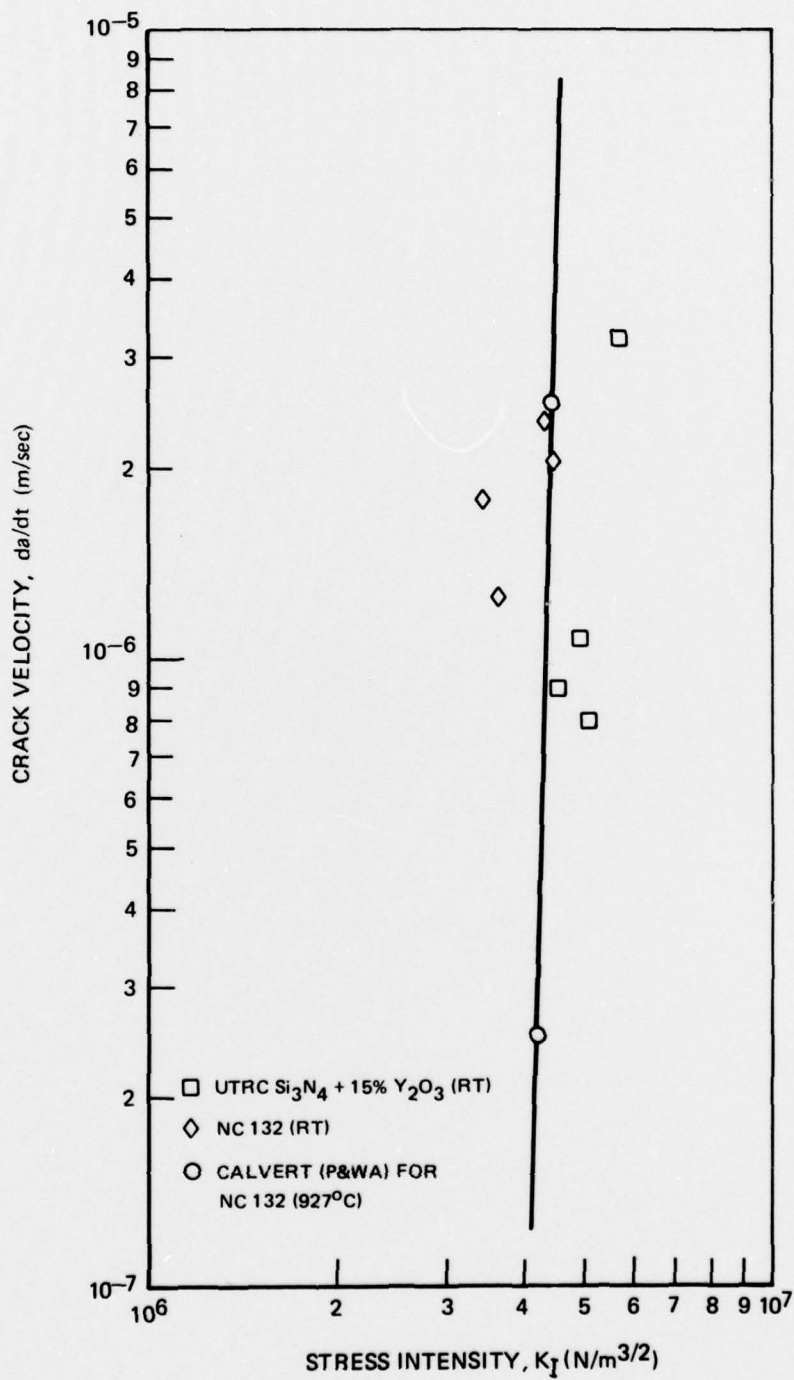


FIG. 27 - X-RADIOGRAPH OF Si_3N_4 -Ta DOUBLE TORSION SAMPLE TESTED AT RT (TOP VIEW)

2x ACTUAL SIZE

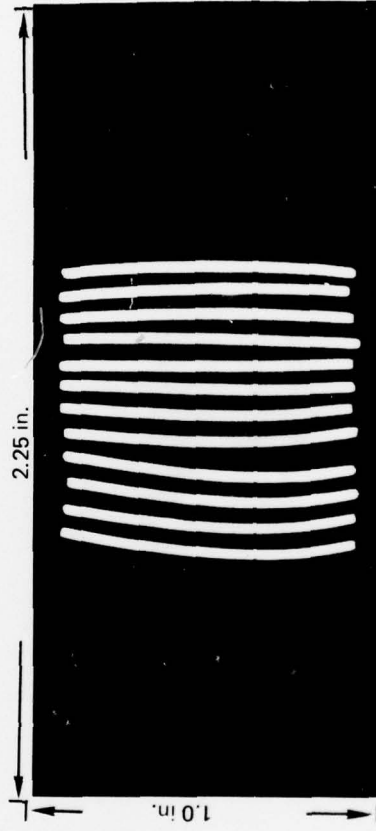
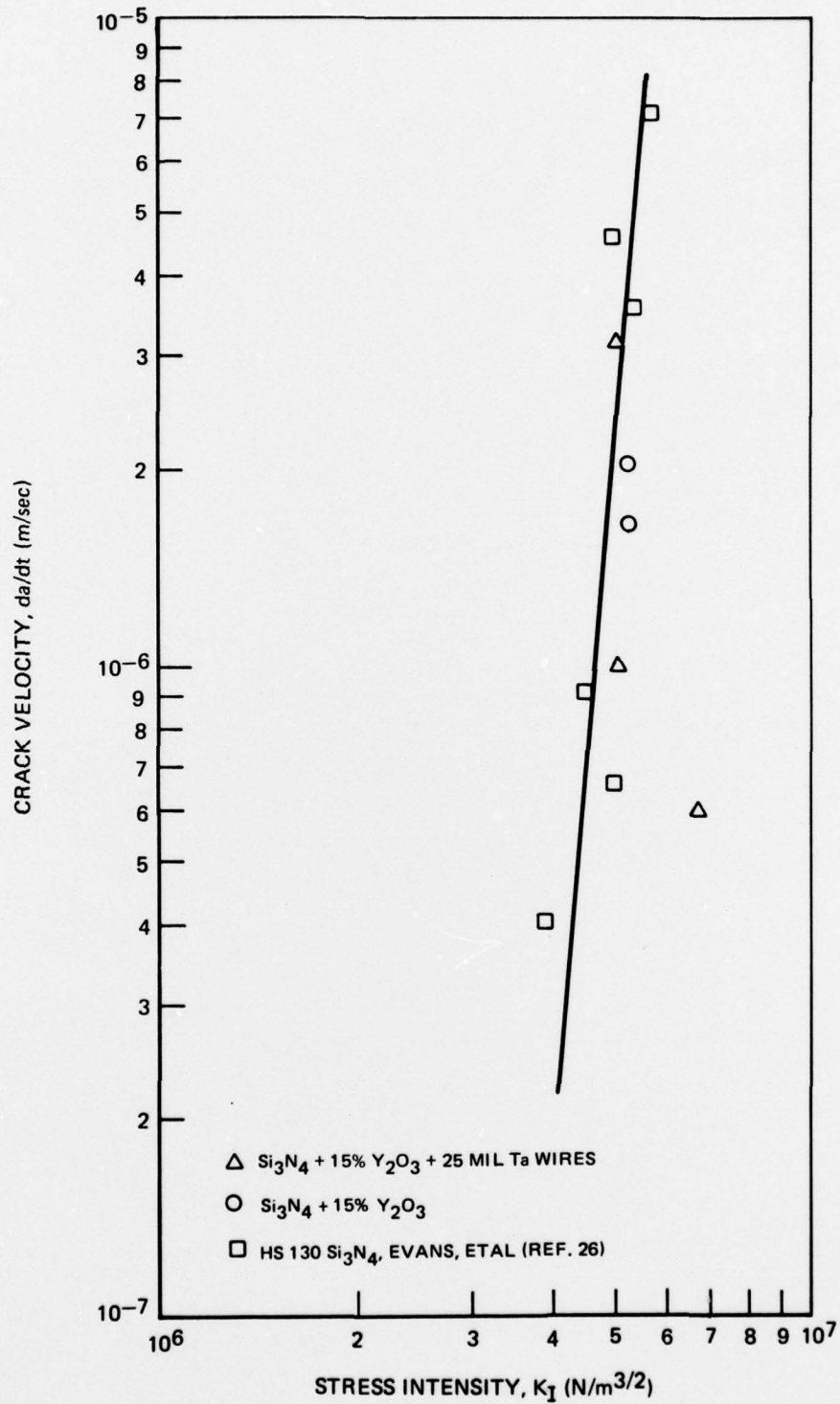


FIG. 28—STRESS INTENSITY VS. CRACK GROWTH RATE FOR Si_3N_4 AND $\text{Si}_3\text{N}_4\text{-Ta}$ AT 1300°C



APPENDIX

Tensile Testing of Ceramics

Special efforts were made at UTRC to ensure that no bending stresses were present during tensile testing. A special jig was made for initially grinding the samples to size with the center of the gage area exactly centered in line with the axes of the holes drilled for the loading pins located at the opposite ends of the samples. The reduced gage section was prepared by plunge grinding four consecutive times into a rectangular sample bar using a 3 in. diameter diamond wheel with 320 grit. Between each of these grinding operations, the sample was rotated 90° around its longest axis and repositioned using a rosin-beeswax cement on a removable metal support plate which could be precisely repositioned on the main metal jig. Holes for the loading pins were made ultrasonically using replaceable drill bushings which were also precisely positioned on the main fixture.

After the samples were prepared, strain gages were mounted on all four opposite faces of the gage section as shown in the attached figure. When the samples were subsequently placed under load in the testing system, the outputs of the strain gages mounted on opposite faces provided a sensitive measure of bending strains and also the optimum test conditions which would eliminate the unequal loadings.

The loading system consisted of two solid 1.25 in. diameter molybdenum studs which were connected to each end of the sample by double pivoted molybdenum yokes with solid tungsten pins. The other ends of these loading studs (cold ends) were attached at the machine crossheads through ball universals mounted in special holders with adjustment screws which permitted lateral adjustments of 0.5 in. in any direction at each crosshead. These adjustments were used for final removal of unequal loadings measured with the strain gages in the gage section prior to test.

Sample alignment for elevated temperature testing was similar to that used for room temperature testing except that the gages were removed with a solvent at room temperature prior to heating and testing. Once good alignment was established, a load holding system was employed to ensure that the alignment was not changed during gage removal or during heating of the sample to the testing temperature.

DISTRIBUTION LIST

(One copy unless otherwise noted)

(3 copies plus balance after distribution)

U.S. Naval Air Systems Command
AIR-52031B
Dept. of the Navy
Washington, DC 20361

(7 copies, for internal distribution by AIR-954, as follows:)

AIR-954 (2 copies), AIR-536B1 (1 copy), AIR-330A (1 copy), AIR-330B
(1 copy), AIR-5361A (1 copy), AIR-5362A (1 copy)
U.S. Naval Air Systems Command
AIR-954
Dept. of the Navy
Washington, DC 20361

(2 copies)

Commander, Naval Air Development Center
Code 302A, A. Fletcher (1 copy)
Code 30232, E. Tankins (1 copy)
Warminster, PA 18974

U.S. Naval Air Turbine Test Station (2 copies)

Attn: J. Glatz (PE-43) (1 copy) A. Martino (AT-1) (1 copy)
1440 Parkway Ave.
Trenton, NJ 08628

U.S. Naval Sea Systems Command

Code 035
Dept. of the Navy
Washington, DC 20362

Commander

Naval Weapons Center
Code 5516
China Lake, CA 93555

U.S. Naval Ships Eng. Center

Code 6146
Dept. of the Navy
Center Bldg., Prince George's Center
Hyattsville, MD 20782

DISTRIBUTION LIST

Naval Weapons Laboratory
Attn: W. Mannschreck
Dahlgren, VA 22448

U.S. Naval Ships Res. & Dev. Center
Code 2812
Annapolis, MD 21402

Naval Surface Weapons Center
Metallurgy Div.
White Oak
Silver Spring, MD 20910

(2 copies)
Director, Naval Research Laboratory
Code 6130 (1 copy)
Code 6360 (1 copy)
Washington, DC 20390

Office of Naval Research
The Metallurgy Program
Code 471
Arlington, VA 22217

Director
Army Materials & Mechanics Res. Center
A. Gorum
Watertown, MA 02172

U.S. Army Aviation Material Labs
Fort Eustis, VA 23604

(2 copies)
Air Force Materials Laboratory
Code LL - H. M. Burte (1 copy)
Code MBC, T. J. Reinhart (1 copy)
Wright-Patterson AFB
Ohio 45433

Air Force Aero Propulsion Laboratory
Code TBP
Wright-Patterson AFB
Ohio 45433

DISTRIBUTION LIST

National Aeronautics & Space Adm.
Code RWM
Washington, DC 20546

(4 copies)
NASA-Lewis Research Center
G. M. Ault (1 copy)
H. P. Probst (1 copy)
W. A. Sanders, MS 49-1 (1 copy)
J. Weeton (1 copy)
21000 Brookpark Road
Cleveland, OH 44135

U.S. Energy Res. & Dev. Adm.
Div. of Reactor Development
A. Van Echo
Washington, DC 20545

Metals & Ceramics Information Center
Battelle Memorial Institute
505 King Avenue
Columbus, OH 43201

The Johns Hopkins Univ.
Applied Physics Laboratory
Maynard L. Hill
8621 Georgia Ave.
Silver Spring, MD 20910

AVCO RAD
201 Lowell St.
Wilmington, MA 01887

IIT Research Institute
10 West 35th St.
Chicago, IL 60616

Detroit Diesel Allison Div.
General Motors Corp.
Materials Laboratories
Indianapolis, IN 46206

DISTRIBUTION LIST

Pratt and Whitney Aircraft Division
United Technologies Corporation
East Hartford, CT 06108

Pratt and Whitney Aircraft
Mr. A. Magid
Government Products Division
West Palm Beach, FL 33402

Chief, Materials Eng. Dept.
Dept. 93-39M
Airesearch Mfg. Co. of Arizona
402 S. 36th St.
Phoenix, AZ 85034

Lycoming Div.
AVCO Corp.
Stratford, CT 06497

Curtis Wright Co.
Wright Aeronautical Div.
Wood-Ridge, NJ 07075

Bell Aerosystems Co.
Technical Library
P.O. Box 1
Buffalo, NY 14240

General Electric Co.
Aircraft Engine Group
Materials & Processes Technology Labs
Evendale, OH 45215

Solar
Dr. A. Metcalfe
2200 Pacific Highway
San Diego, CA 92112

Teledyne CAE
1330 Laskey Road
Toledo, OH 43601

DISTRIBUTION LIST

Stellite Div.
Cabot Co.
Technical Library
P.O. Box 746
Kokomo, IN 46901

(2 copies)
General Electric Co.
Corporate Res. & Dev.
Attn: W. Hillig (1 copy)
R. Charles (1 copy)
P.O. Box 8
Schenectady, NY 12301

Norton Co.
Protective Products Div.
Attn: N. J. Ault
Worcester, MA 01606

Westinghouse Electric Co.
Materials & Processing Laboratory
Attn: R. Bratten
Beulah Road
Pittsburgh, PA 15235

Westinghouse Electric Co.
Lester Branch 9175
Attn: A. N. Holden
Philadelphia, PA 19113

The Carborundum Co.
Niagara Falls, NY 14302

Ford Motor Co.
Product Development Group
Attn: E. A. Fisher
2000 Rotunda Drive
Dearborn, MI 48121

General Electric Co.
AEGT Technical Information Center
Mail Drop N-32, Bldg. 700
Cincinnati, OH 45215

DISTRIBUTION LIST

Prof. R. E. Tressler
Ceramic Science Section
Pennsylvania State Univ.
201 Mineral Industries Bldg.
University Park, PA 16802

Dr. T. D. Chikalla
Ceramics & Graphite Section
Battelle-Northwest
Richland, WA 99352

TRW Equipment Laboratories
23555 Euclid Ave.
Cleveland, OH 44117

Final Report Only (12 copies)

Commander
Naval Air Development Center
Code 302A, A. Fletcher for DDC
Warminster, PA 18974

Final Report Only (3 copies)

Commander
Naval Air Development Center
Code 813
Warminster, PA 18974